Title

Tracheal Separation is Driven by NKX2-1-Mediated Repression of *Efnb2* and Regulation of Endodermal Cell Sorting

Authors

Lewis, Ace
Kuwahara, Akela
Franzosi, Jacqueline
et al.

Publication Date

2022-12-21

Peer reviewed

HHS Public Access

Author manuscript

Cell Rep. Author manuscript; available in PMC 2022 April 22.

Published in final edited form as:

Cell Rep. 2022 March 15; 38(11): 110510. doi:10.1016/j.celrep.2022.110510.

Tracheal separation is driven by NKX2-1-mediated repression of *Efnb2* and regulation of endodermal cell sorting

Ace E. Lewis[1,2,3,4], **Akela Kuwahara**[1,2,3,4,5], **Jacqueline Franzosi**[1,2,3,4], **Jeffrey O. Bush**[1,2,3,4,6,*]

[1]Department of Cell and Tissue Biology, University of California, San Francisco, San Francisco, CA 94143, USA

[2]Program in Craniofacial Biology, University of California, San Francisco, 513 Parnassus Avenue, Box 0512, San Francisco, CA 94143, USA

[3]Institute for Human Genetics, University of California, San Francisco, San Francisco, CA 94143, USA

[4]Eli and Edythe Broad Center of Regeneration Medicine and Stem Cell Research, University of California, San Francisco, San Francisco, CA 94143, USA

[5]Developmental and Stem Cell Biology Graduate Program, University of California, San Francisco, San Francisco, CA 94143, USA

[6]Lead contact

SUMMARY

The mechanisms coupling fate specification of distinct tissues to their physical separation remain to be understood. The trachea and esophagus differentiate from a single tube of definitive endoderm, requiring the transcription factors SOX2 and NKX2-1, but how the dorsoventral site of tissue separation is defined to allocate tracheal and esophageal cell types is unknown. Here, we show that the EPH/EPHRIN signaling gene *Efnb2* regulates tracheoesophageal separation by controlling the dorsoventral allocation of tracheal-fated cells. Ventral loss of NKX2-1 results in disruption of separation and expansion of *Efnb2* expression in the trachea independent of SOX2. Through chromatin immunoprecipitation and reporter assays, we find that NKX2-1 likely represses *Efnb2* directly. Lineage tracing shows that loss of NKX2-1 results in misallocation of ventral foregut cells into the esophagus, while mosaicism for *NKX2-1* generates ectopic NKX2-1/EPHRIN-B2 boundaries that organize ectopic tracheal separation. Together, these data

*Correspondence: jeffrey.bush@ucsf.edu.

AUTHOR CONTRIBUTIONS

Conceptualization, A.E.L. and J.O.B.; methodology, A.E.L. and J.O.B.; validation, A.E.L., A.K., and J.F.; formal analysis, A.E.L., A.K., and J.O.B.; investigation, A.E.L., A.K., and J.F.; writing – original draft, A.E.L., A.K., and J.O.B.; writing – review & editing, A.E.L., A.K., J.F., and J.O.B.; visualization, A.E.L.; supervision, A.E.L. and J.O.B.; project administration, A.E.L. and J.O.B.; funding acquisition, A.E.L., A.K., and J.O.B.

DECLARATION OF INTERESTS

The authors declare no competing interests.

SUPPLEMENTAL INFORMATION

Supplemental information can be found online at https://doi.org/10.1016/j.celrep.2022.110510.

demonstrate that NKX2-1 coordinates tracheal specification with tissue separation through the regulation of EPHRIN-B2 and tracheoesophageal cell sorting.

In brief

Lewis et al. show that, in the development of the mammalian trachea and esophagus, cell fate specification is coupled with morphogenesis by NKX2-1-mediated repression of *Efnb2*. This establishes an EPH/EPHRIN boundary that drives cell allocation and physical separation of the trachea and esophagus.

Graphical Abstract

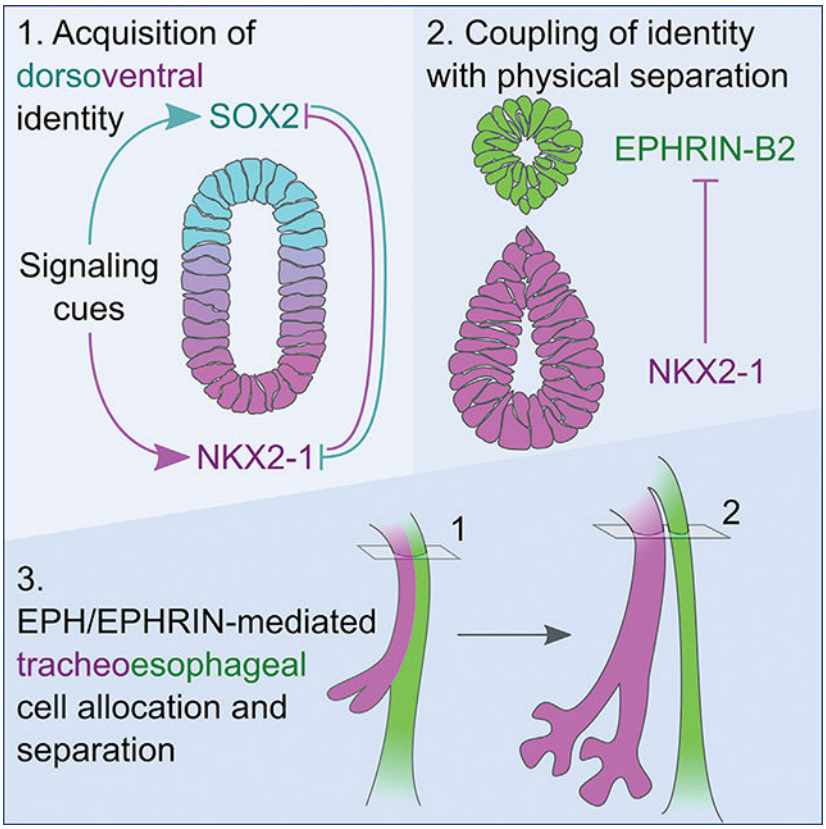

INTRODUCTION

During early organogenesis, transcriptional patterning of distinct tissues often precedes their physical separation into organs and tissues, but our understanding of how transcriptional cell fate specification programs couple to physical morphogenesis is limited. The mammalian trachea and esophagus are both derived from a single tube of definitive foregut endoderm, which requires multiple signals from the surrounding splanchnic mesoderm to induce differential dorsoventral transcriptional programs that specify tracheal and esophageal cell fates. The adult trachea consists of a pseudostratified columnar epithelium interspersed with ciliated and secretory cells and surrounded ventrally by cartilaginous rings, whereas the esophagus is composed of stratified squamous epithelium surrounded by smooth muscle.

Expression of the transcription factor NKX2-1 (TTF1) in the early ventral foregut endoderm marks the future lung and trachea, while high expression of SOX2 in the dorsal endoderm marks the future esophagus (Guazzi et al., 1990; Minoo et al., 1999; Mizuno et al., 1991; Que et al., 2007). After their specification, the trachea and esophagus must separate; their failure to do so results in the common human congenital anomalies tracheoesophageal fistula (TEF) and tracheal agenesis (Billmyre et al., 2015; Morrisey and Hogan, 2010; Sher and Liu, 2016). In mice, loss of *NKX2-1* results in dramatic dysmorphology of the lung and failure to form a trachea, with upregulation of SOX2 in the ventral endoderm (Goss et al., 2009; Harris-Johnson et al., 2009; Minoo et al., 1999; Que et al., 2007). Surprisingly, our recent RNA sequencing (RNA-seq) studies indicate that NKX2-1 regulates a relatively small subset of genes that are differentially expressed between the trachea and esophagus during early development, indicating that, at this stage, relatively few key targets may be responsible for mediating these phenotypes (Kuwahara et al., 2020). Hypomorphic reduction of SOX2 expression also results in failure of tracheoesophageal (TE) separation with increased expression of NKX2-1 in the dorsal endoderm (Que et al., 2007). Therefore, NKX2-1 and SOX2 form a dual repressive regulatory circuit that is critical for TE development, though downstream transcriptional targets that mediate TE separation are currently unknown.

Beyond molecular regulation, even the morphogenetic and cellular mechanisms by which TE separation occurs are incompletely understood, and how the dorsoventral position of separation is defined is unknown. TE separation begins at the lung buds and proceeds rostrally, separating the trachea and esophagus until reaching the pharynx. Though it was proposed that differential outgrowth of the trachea and/or distal esophagus drive their formation (Sasaki et al., 2001; Zaw-Tun, 1982), subsequent studies showed that the unseparated part of the foregut tube decreases in absolute length over the course of its development, indicating that formation of the trachea and esophagus involves active separation of one tube into two, rather than proliferative growth of the trachea from the foregut endoderm (Ioannides et al., 2010). Live imaging of separation in cultured foreguts suggested an inclusive “splitting and extension model” in which localized airway and esophageal growth distal to the point of TE separation is coordinated with the rostral movement of a saddle-like structure (Que, 2015). More recently, a model has been posited in which mesenchyme at the lateral sides of the foregut pushes medially to generate a septum and progressively pinch off the trachea from esophageal lumen (Nasr et al., 2019), but how the site of separation is precisely determined and coupled to TE fate specification is not clear.

EPH/EPHRIN signaling is a major regulator of morphogenesis and tissue separation in many developmental contexts, including the hindbrain rhombomeres, mesodermal somites, hepatopancreatic duct, and pharyngeal endoderm (Choe and Crump, 2015; Cooke et al., 2001; Jülich et al., 2009; Thestrup et al., 2019; Xu et al., 1995, 1999). The EPH receptor tyrosine kinases signal bidirectionally in partnership with their cognate, membrane-bound EPHRINS to regulate a wide range of cellular behaviors, including migration, proliferation, and apoptosis, in a host of systems (Kania and Klein, 2016; Pasquale, 2005). Often, this signaling family impacts morphogenesis by regulating cellular position through cell sorting, in which EPH-expressing cells separate from EPHRIN-expressing cells to self-organize

(Cayuso et al., 2015; Niethamer and Bush, 2019; O'Neill et al., 2016; Xu et al., 1999). Interestingly, we and others have previously shown that loss of function of the *Efnb2* gene, which encodes EPHRIN-B2, results in a failure of TE separation, though the developmental and cellular mechanisms remain unknown, and it is unclear how *Efnb2* is regulated (Dravis and Henkemeyer, 2011; Lewis et al., 2015).

Here, we show that EPHRIN-B2 is a key effector that couples cell fate specification with physical separation of the trachea and esophagus. Whereas EPHRIN-B2 loss does not affect early dorsoventral patterning of the foregut, we find that EPHRIN-B2 is required within the dorsal endoderm for the dorsoventral allocation of tracheal-fated cells at the site of separation and for the separation of the trachea from the esophagus. Further, we find that NKX2-1, a regulator of respiratory cell fate, directly binds to the *Efnb2* gene to repress its transcription. The repression of *Efnb2* by NKX2-1 creates a sharp boundary that defines the point of tissue separation. Notably, ectopic NKX2-1/EPHRIN-B2 expression boundaries result in ectopic tracheal separation, indicating that this boundary determines the position of tracheal separation. Whereas we find that SOX2 is not required for *Efnb2* expression, SOX2 expression at the dorsoventral interface is required for induction of TE separation at NKX2-1/EPHRIN-B2 boundaries. Together, these results unveil the mechanism by which dorsoventral position and tracheoesophageal fate specification are coupled to the proper spatial allocation of distinct cell fates and to the physical separation of the trachea and esophagus.

RESULTS

Endodermal EPHRIN-B2 is required for TE separation to establish the dorsoventral foregut boundary

To better understand the function of EPHRIN-B2 in TE development, we detailed the expression pattern of the *Efnb2* gene before, during, and after TE separation using a knockin reporter allele that expresses H2B-GFP from the endogenous *Efnb2* locus and disrupts EPHRIN-B2 function. At embryonic day 9.5 (E9.5), prior to separation, we observed high levels of GFP reporter expression in the dorsal foregut endoderm, with notably reduced expression in the ventral foregut endoderm (Figures S1A and S1D). At E10.5, when TE separation is underway, endodermal GFP expression was restricted to the dorsal domain of unseparated regions of the foregut and to the newly separated esophagus but was absent from the tracheal endoderm (Figures S1F and S1I). Following complete TE separation at E11.5, GFP was detected in the esophageal endoderm but was notably absent from the tracheal endoderm (Figures S1K and S1N). At all three stages, *Efnb2* reporter expression in the dorsal endoderm was complementary to the tracheal marker NKX2-1 and overlapped with high levels of SOX2 expression (Figures S1A–S1O). GFP expression was also detected throughout the foregut mesenchyme and within the adjacent vascular endothelium at all three stages, as previously reported (Davy and Soriano, 2007; Dravis and Henkemeyer, 2011; Wang et al., 1998).

Because widespread loss of EPHRIN-B2 results in embryonic lethality at E9.5 due to failure of angiogenic remodeling (Wang et al., 1998), we previously established a conditional rescue strategy wherein widespread *Efnb2* loss of function is conditionally restored

specifically within the vascular endothelium by crossing to Tie2-Cre mice (Braren et al., 2006), hereafter referred to as *Efnb2*^{CR} (Lewis et al., 2015). We combined this strategy with the *Efnb2*$^{H2B\text{-}GFP}$ reporter allele to track the *Efnb2* expression pattern in the absence of functional *Efnb2*. To begin to understand the morphological basis of the TEF phenotype upon loss of EPHRIN-B2, we created 3D reconstructions of E15.5 *Efnb2*$^{CR/H2B\text{-}GFP}$ mutant foreguts and confirmed a failure of TE separation with complete penetrance as well as an overall shorter foregut compared with controls (Figures 1A and 1B).

Based on the observation that the dorsoventral boundary of *Efnb2*$^{H2B\text{-}GFP}$ reporter expression demarcates the position of TE separation (Figures S1A, S1D, S1F, and S1I), we next asked whether its conditional disruption within the endoderm results in a TEF phenotype by using a tamoxifen-inducible Cre recombinase expressed from the *Sox2* locus (Arnold et al., 2011). Following tamoxifen induction at E7.5 and E8.5, we observed that recombination in E10.5 *Sox2*$^{CreER/+}$; *ROSA26*$^{LacZ/+}$ embryos was abundant in the esophageal-fated endoderm, mostly absent from tracheal-fated endoderm, and completely absent from the foregut mesenchyme (Figure 1C). Using the same tamoxifen regimen, we observed a TEF phenotype in E11.5 *Efnb2*$^{lox/lox}$; *Sox2*$^{CreER/+}$ mutant embryos, but not in *Efnb2*$^{lox/+}$; *Sox2*$^{CreER/+}$ littermates (Figures 1D and 1E), indicating that the dorsal endodermal expression of EPHRIN-B2 is required for TE separation to occur.

Localized differences in cell proliferation and cell death in the foregut endoderm have been proposed to contribute to TE separation (Billmyre et al., 2015; Que, 2015), so we quantified cell proliferation by bromodeoxyuridine (BrdU) incorporation assay and apoptosis by cleaved caspase-3 immunostaining in E10.5 *Efnb2*$^{CR/H2B\text{-}GFP}$ embryos compared with wild-type littermates. We did not observe a significant difference in the percentage of BrdU-positive cells or in the extent of cleaved caspase3 staining between mutant and control foregut endoderm at any position along the rostrocaudal axis (Figure S2), indicating that the *Efnb2* mutant TEF phenotype is not likely attributable to differences in cell proliferation or apoptosis.

Because other genetic models of TEF frequently show a loss or conversion of dorsoventral endoderm identity (Billmyre et al., 2015), we sought to determine whether loss of *Efnb2* was also impacting fate determination. Immunostaining revealed that, despite the failure of TE separation, E11.5 *Efnb2*$^{CR/H2B\text{-}GFP}$ mutant embryos exhibited dorsally enriched SOX2 expression as well as ventrally restricted NKX2-1 expression perfectly apposed to *Efnb2*$^{H2B\text{-}GFP}$ reporter expression, similar to controls (Figures 1F–1O). These data indicate that EPHRIN-B2 does not control foregut dorsoventral fate specification and that its loss does not perturb TE separation by this mechanism.

To better understand how EPHRIN-B2 signaling regulates TE separation, we examined the expression of its six cognate receptor genes. Though EPHB2 and EPHB3 expression has previously been examined in this context, their compound disruption does not result in failed TE separation and the expression of other EPH receptors in the foregut is currently unknown (Dravis and Henkemeyer, 2011). RNA-seq of the trachea and esophagus in wild-type E11.5 embryos revealed high expression of *Ephb2*, *Ephb3*, Ephb4, and *Epha4* in both the foregut endoderm and mesenchyme, whereas *Ephb1* and *Ephb6* displayed

low expression and were discounted from further analyses (Figure S3A; Kuwahara et al., 2020). We examined the spatial patterns of expression of *Ephb2*, *b3*, *b4*, and *a4* through *in situ* hybridization by RNAScope on wild-type sections at E10.5 and E11.5 and by immunofluorescence on $Efnb2^{H2B\text{-}GFP/+}$ mutant embryo sections at E10.5 and found that indeed all of these exhibited expression in both the endoderm and mesenchyme (Figures S3B–S3M'). Whereas most were expressed broadly, we found that EPHA4 exhibited ventrally enriched endodermal expression at E10.5, though this expression did not extend far enough dorsally to contact the EPHRIN-B2 expression domain (Figures S3B and S3J). Each of the receptors except EPHB2 also exhibited elevated mesenchymal expression adjacent to the lateral edges of the foregut (stars in Figures S3J, S3L, and S3M). To clarify which domains of EPH receptor expression may be regulating TE separation, we assayed EPH receptor phosphorylation in *Efnb2* mutant and control sections at E11.5. Immunostaining for pan-phosphorylated-EPHB1+B2 and pan-phosphorylated-EPHA2+A3+A4 in controls produced a strikingly greater signal in the foregut endoderm compared with that of the surrounding mesenchyme, suggesting that the relevant signaling interaction with EPHRIN-B2 may involve endodermal EPH receptors (Figures S4D–S4G). EPH receptor phosphorylation appeared to be modestly diminished in the dorsal endoderm of *Efnb2* mutants relative to the esophagus of controls; this is compatible with other findings in which EPH and EPHRIN co-expressing cells are believed to signal with each other within the same domain (Bush and Soriano, 2010; Dravis and Henkemeyer, 2011) and suggests that signaling to receptors in the EPHRIN-B2-expressing domain may be of particular relevance (Figures S3B and S3D).

It has been reported that *Epha4; Ephb1; Ephb2; Ephb3* compound mutant mice do not exhibit a TEF phenotype (Dravis and Henkemeyer, 2011), leaving EPHB4 as a likely candidate factor. As EPHRIN-B2 is a known binding partner of EPHB4, which exhibits parallel loss-of-function phenotypes in angiogenesis that prevent analysis of its role in foregut development (Chrencik et al., 2006; Gerety et al., 1999; Wang et al., 1998), we performed endodermal deletion of *Ephb4* within the foregut endoderm using the *Gata4-G4-Cre* allele, which exhibits highly efficient recombination by E10.5 (Figures S4H and S4I). Near complete loss of EPHB4 in the endoderm of $Ephb4^{lox/lox}$; $Gata4\text{-}G4\text{-}Cre^{Tg/+}$ embryos did not disrupt TE separation (Figures S4J and S4K), however, indicating that EPHB4 is required in the mesenchyme and/or that functional redundancy between multiple EPH receptors is at play.

As the $Sox2^{CreER}$ mouse line described above is haploinsufficient for *Sox2* function, and because SOX2 dosage sensitivity has been previously demonstrated in TE separation (Que et al., 2007), we turned to another endoderm-specific Cre mouse line for further studies. Using a tamoxifen-inducible Cre recombinase knocked into the *Foxa2* locus with a single injection of tamoxifen at E6.5, we were able to achieve a high percentage of recombination in the foregut endoderm as shown by $ROSA26^{Ai75}$ reporter expression (Figure S4A; Park et al., 2008). As expected, $Efnb2^{lox/lox}$; $Foxa2^{CreER/+}$ mutant embryos exhibited a TEF phenotype with correct dorsoventral patterning as marked by NKX2-1 and SOX2, phenocopying the foreguts of $Efnb2^{CR/H2B\text{-}GFP}$ mutants (Figures S4B and S4C). Three-dimensional renderings of immunostaining for NKX2-1 and E-cadherin in whole dissected $Efnb2^{lox/lox}$; $Foxa2^{CreER/+}$ mutant and control foreguts at E10.5 revealed that the

TEF phenotype is evident from the earliest time at which TE separation begins (Figures 2A–2B', orange arrowheads). Interestingly, whereas NKX2-1-positive cells were not found dorsal to the TE saddle region in control embryos, they were found ectopically positioned in the distal esophagus and dorsal unseparated foregut of mutant embryos (Figures 2A–2B', white arrows). These results indicate endodermal EPHRIN-B2 expression regulates separation morphogenesis, possibly by maintaining correct tracheal cell positioning.

Loss of EPHRIN-B2 results in misallocation of tracheal cells into the esophagus

Recent findings indicate that relatively few *NKX2-1* lineage cells contribute to the esophagus normally, which we confirmed by performing lineage tracing in *NKX2-1*$^{CreER/+}$;*ROSA26*$^{LacZ/+}$ embryos at E11.5, following TE separation (Figures S5A; Kim et al., 2019). Given our above finding that loss of EPHRIN-B2 permits the aberrant mixing of tracheal-fated cells into the esophagus, we examined the consequences of this early misallocation later, at E14.5, by immunostaining for NKX2-1 compared with LRIG1, which we recently identified as a marker of early esophageal endoderm (Guazzi et al., 1990; Kuwahara et al., 2020; Mizuno et al., 1991). Control sections exhibited no NKX2-1-expressing cells within the esophagus, while LRIG1 displayed high expression in the basal esophageal epithelium, lower expression in the apical esophageal epithelium, and no expression in the tracheal epithelium (Figures 2C–2D"). However, we found numerous NKX2-1-positive cells inappropriately intermixed within the dorsal endoderm of E14.5 *Efnb2*$^{lox/lox}$; *Foxa2*$^{CreER/+}$ mutant embryos (Figures 2E–2E"). Ectopically positioned NKX2-1-positive cells exhibited low, or no, LRIG1 expression compared with dorsal NKX2-1-negative cells, which expressed comparatively high LRIG1 (Figures 2E–2E", arrows). We also consistently observed ectopic NKX2-1-positive cells contributing to the esophagus immediately distal to the fistula in *Efnb2*$^{lox/lox}$; *Foxa2*$^{CreER/+}$ mutant embryos (magenta arrows in Figures 2F–2F"). As in the fistula, LRIG1 expression in these regions was generally lower or absent and epithelial stratification was disorganized, though the basal localization of LRIG1-positive cells was overtly maintained. More caudally, we found diminishing numbers of misallocated NKX2-1-positive cells as well as normal LRIG1 cell localization and epithelial stratification (Figures 2G–2G"). Interestingly, the position of TE separation failure in *Efnb2*$^{lox/lox}$; *Foxa2*$^{CreER/+}$ mutant embryos was immediately rostral to the misallocated tracheal cells, suggesting that TE cell allocation and separation are linked (Figures 2E–2G).

Given this apparent misallocation of ventral cells into the dorsal foregut of *Efnb2* mutants, we next sought to discern the consequences of *Efnb2* loss upon later tracheal and esophageal organogenesis. Histological sections of the distal trachea in E18.5 *Efnb2*$^{CR/H2B\text{-}GFP}$ mutant embryos revealed a layer of tall columnar cells ventrally and a layer of shorter columnar cells dorsally, comparable to control tracheae (Figures 3Aa, 3Ab, 3Be, and 3Bf). Whereas the dorsal region of the *Efnb2*$^{CR/H2B\text{-}GFP}$ mutant distal esophagus exhibited squamous epithelial architecture similar to control (Figures 3Ac and 3Bg), the ventral region of the *Efnb2*$^{CR/H2B\text{-}GFP}$ mutant distal esophagus exhibited an apical layer of cells that, unlike in control (Figure 3Ad), was not squamous but rather more tracheal with a taller columnar appearance (Figure 3Bh). Similarly, ventral regions of the unseparated mutant foregut appeared columnar (Figure 3Cj) and dorsal regions appeared stratified squamous (Figure

3Ci), whereas lateral regions lacked squamous layers but instead contained more columnar apical cells over a basal layer of cuboidal cells (Figures 3Ck and 3Cl).

Based on these histological findings, we examined the distribution of tracheal and esophageal cell types in E18.5 *Efnb2*$^{CR/H2B\text{-}GFP}$ mutant embryos using immunostaining. As expected, control tracheae contained ciliated cells expressing acetylated α-tubulin and mucinous cells expressing MUC5B and displayed broad KRT8 expression accompanied by sparse KRT5-positive basal cells; control esophagi exhibited more abundant KRT5 basal epithelial cells accompanied by sparse KRT8-positive apical cells (Figures 3D–3I). Whereas the distal trachea in *Efnb2*$^{CR/H2B\text{-}GFP}$ mutants exhibited identical marker expression to control tracheae (Figures 3M–3O), the esophagus immediately distal to the fistula exhibited ectopic localization of multiple NKX2-1-expressing tracheal cell types, including multi-ciliated, mucinous, and KRT8-expressing cells (Figures 3J–3L). Combined, these data indicate that, upon loss of EPH-RIN-B2, misallocated NKX2-1-expressing cells within the dorsal foregut differentiate into ectopically localized tracheal cell types within the dorsal unseparated foregut and distal esophagus.

Efnb2 is bound and repressed by NKX2-1 but is independent of SOX2 regulation

As loss of EPHRIN-B2 did not influence the early dorsoventral patterning of the foregut, and because its expression did faithfully mark only the dorsal, presumptive esophageal endoderm, we hypothesized that the expression of *Efnb2* might be under the control of known components of the dorsoventral patterning program in the foregut. As NKX2-1 and SOX2 are known regulators of this program (Domyan et al., 2011; Kuwahara et al., 2020; Minoo et al., 1999; Que et al., 2007), we disrupted their expression within the foregut endoderm to examine the effects on *Efnb2* patterning. As previously reported, loss of NKX2-1 resulted in a TEF phenotype with ventral upregulation of SOX2 in *NKX2-1*$^{lox/lox}$*; Foxa2*$^{CreER/+}$*; Efnb2*$^{H2B\text{-}GFP/+}$ mutant E11.5 embryos compared with control (Figures 4A, 4B, 4E, and 4F; Harris-Johnson et al., 2009; Kuwahara et al., 2020; Que et al., 2007). We additionally observed ventral upregulation of *Efnb2*$^{H2B\text{-}GFP}$ reporter expression in the same cells that exhibited upregulation of SOX2 (Figures 4C, 4D, 4G, and 4H). Conversely, loss of SOX2 resulted in a TEF with upregulation of dorsal expression of NKX2-1 and complete loss of *Efnb2*$^{H2B\text{-}GFP}$ reporter expression in *Sox2*$^{lox/lox}$*; Foxa2*$^{CreER/+}$*; Efnb2*$^{H2B\text{-}GFP/+}$ mutant E11.5 embryos (Figures 4I–4L). These data indicate that *Efnb2* is indeed under control of the NKX2-1/SOX2 dorsoventral program but do not reveal whether NKX2-1 represses *Efnb2*, whether SOX2 activates *Efnb2*, or both.

To disentangle this regulatory relationship, we took advantage of incomplete and overlapping patterns of tamoxifen-mediated recombination to decipher the effects of compound loss of NKX2-1 and SOX2, individually and in combination, on *Efnb2* expression using *NKX2-1*$^{lox/lox}$*; Sox2*$^{lox/lox}$*; Foxa2*$^{CreER/+}$*; Efnb2*$^{H2B\text{-}GFP/+}$ mutant E11.5 embryos. In all samples, we found that regions lacking either transcription factor individually exhibited *Efnb2*$^{H2B\text{-}GFP}$ reporter expression consistent with individual mutants; loss of both NKX2-1 and SOX2 in the same cells resulted in a persistence of *Efnb2*$^{H2B\text{-}GFP}$ reporter expression, such that all endoderm cells always expressed either NKX2-1 or Efnb2 and not both, regardless of SOX2 expression (Figures 4M–4P). Taken together,

these genetic data indicate that *Efnb2* expression is restricted to the dorsal endoderm by NKX2-1-mediated repression in the ventral endoderm and does not involve transcriptional activation by SOX2.

Based on these genetic findings, we sought to ask whether NKX2-1 might directly repress *Efnb2* expression in the ventral foregut. Our lab recently reported an NKX2-1 chromatin immunoprecipitation (ChIP)-seq dataset from E11.5 foreguts (Kuwahara et al., 2020), which we queried to determine whether NKX2-1 binds near the *Efnb2* locus. We identified several NKX2-1-binding sites at the *Efnb2* locus: one site 200 kb up-stream of *Efnb2*, one site at the *Efnb2* promoter, one site within the first intron of the *Efnb2* gene, and two sites 30 kb and 55 kb downstream of *Efnb2* (Figure 4Q). We selected four peaks with statistically significant enrichment in both NKX2-1 ChIP-seq replicates (MACS2 peak calling; false discovery rate [FDR] < 0.00001) and confirmed them by ChIP-PCR for NKX2-1 in E11.5 foreguts. In two ChIP-PCR replicates, all four peaks exhibited significantly enriched NKX2-1 binding compared with control immunoglobulin G (IgG) and to a negative control genomic region (Figure 4R). Together with the above genetic data, these results indicate that NKX2-1 binds directly to the *Efnb2* locus in the foregut epithelium and that loss of NKX2-1 de-represses *Efnb2* expression.

To assess the functional significance of NKX2-1 binding at these putative silencer regions (SRs), we performed luciferase assays using MLE-15 cells, which are derived from distal mouse lung epithelium and known to express NKX2-1 (Bruno et al., 1995; Wikenheiser et al., 1993). Reporter constructs were prepared by inserting individually and in tandem each SR identified above as well as the promoter region identified in one of the two ChIP-seq biological replicates ahead of either a PGK or TK promoter driving luciferase expression. Transient transfection of MLE-15 cells with each of the above constructs resulted in a decrease of luminescence compared with controls, indicating that each SR indeed acts as a silencer in combination with either promoter (Figures 4S and 4T, dark bars). Insertion of all predicted silencers in tandem ahead of the PGK promoter resulted in the greatest observed decrease of luciferase activity, suggesting combinatorial function in suppression of *Efnb2* expression. We next ablated NKX2-1 binding through substitution of predicted NKX2-1 binding motifs with adenines or thymines as performed previously (Sandberg et al., 2016). Luciferase reporter assays revealed a variable effect of disruption of NKX2-1, which also differed depending on the minimal promoter that was used (Figures 4S and 4T, pale bars). Each SR was able to significantly rescue luciferase activity upon mutation of NKX2-1-binding sites in combination with at least one of the two promoters employed. Indeed, for SR's +646 with the TK promoter and +130 and +845 with the PGK promoter, luciferase activity was fully rescued to the levels of the positive controls (Figures 4S and 4T). In the case of SR's −4 and +646, while a significant rescue of activity was observed with the TK promoter, significantly decreased activity was observed with the PGK promoter, underscoring the limitations of the practice of testing *cis*-regulatory function in exogenous assays. Nevertheless, these data clearly demonstrate that the SRs we have identified can indeed act as transcriptional silencers that depend on NKX2-1 for their activity.

NKX2-1/EPHRIN-B2 boundaries organize the site of TE separation

Having shown that NKX2-1 represses *Efnb2* to establish its dorsally restricted expression pattern and that loss of EPHRIN-B2 results in the misallocation of NKX2-1-positive cells to the dorsal foregut, we next asked whether the primary role of NKX2-1 in TE separation is to establish an EPHRIN-B2 boundary that drives TE tissue separation. To test whether a normally positioned EPHRIN-B2 expression boundary could initiate TE separation in the absence of NKX2-1, we utilized a tamoxifen-inducible Cre recombinase knocked into the *NKX2-1* locus that simultaneously disrupts its function. We observed recombination in $NKX2\text{-}1^{CreER/+}; ROSA26^{LacZ/+}$ embryos that confirmed that Cre activity is almost entirely confined to the tracheal-fated endoderm (Figure S5A), and we confirmed that $NKX2\text{-}1^{CreER/CreER}$ mutant embryos displayed a complete loss of endodermal NKX2-1 that resulted in a TEF phenotype (Figure S5G). We used this allele to generate compound $Efnb2^{lox/lox}; NKX2\text{-}1^{CreER/CreER}$ mutant embryos to simultaneously remove NKX2-1 function and restore the normal dorsoventral EPHRIN-B2 expression boundary. We found that these mutant foreguts did not exhibit restored TE separation (Figure S5H), suggesting that NKX2-1 regulates additional genes that are required to mediate TE separation.

It has been posited that lateral foregut endoderm cells that express both NKX2-1 and SOX2, termed midline epithelial cells (MECs), are crucial for foregut separation (Kim et al., 2019). To test whether EPHRIN-B2 is required at this dorsoventral interface, we deleted *Efnb2* in the cells apposing the NKX2-1 domain by utilizing $Shh^{Cre\text{-}EGFP}$, which at E11.5 exhibits recombination throughout the ventral foregut endoderm encompassing NKX2-1-expressing cells as well as the cells immediately dorsal to them (Figures S5B–S5D; Harfe et al., 2004; Harris-Johnson et al., 2009). As expected, E11.5 $Efnb2^{lox/lox}; Shh^{Cre\text{-}EGFP/+}$ mutant embryos exhibited normal patterns of NKX2-1 and SOX2 expression but, interestingly, also exhibited a TEF phenotype, indicating that EPHRIN-B2 is required within cells at the dorsoventral boundary and in apposition to those expressing NKX2-1 (Figure S5F). Based on the fact that both EPHRIN-B2 and NKX2-1 expression at this interface was necessary but neither was sufficient for TE separation, we tested whether SOX2 is also required at this interface by generating $Sox2^{lox/lox}; Shh^{Cre\text{-}EGFP}$ mutant E11.5 embryos that lack SOX2 expression within and directly dorsal to the NKX2-1 domain (Figures S5I–S5L). These embryos also failed to undergo TE separation, indicating that, whereas SOX2 is not directly required for regulating *Efnb2* expression, it is necessary at the MEC/dorsoventral interface for TE separation to occur.

While observing tamoxifen-generated *NKX2-1* mosaicism, we made the striking discovery that $NKX2\text{-}1^{lox/lox}; Foxa2^{CreER/+}$ mutant foreguts in which recombination of NKX2-1 was incomplete exhibited a robust sorting of NKX2-1-positive and negative cells. Whereas E11.5 $ROSA26^{mTmG/+}; Foxa2^{CreER/+}$ embryos exhibited recombination in a distributed salt-and-pepper mosaic pattern, E11.5 $NKX2\text{-}1^{lox/lox}; Foxa2^{CreER/+}$ mutant embryos exhibited large NKX2-1-positive and negative patches (Figures 5A and 5B). To further confirm that this organization occurred by cell sorting rather than clonal expansion of mosaic recombination domains, we examined cellular organization over the time course of TE separation. Whole dissected E9.75 $NKX2\text{-}1^{lox/lox}; Foxa2^{CreER/+}$ mutant foreguts exhibited mosaic recombination and loss of NKX2-1 distributed in an intermixed salt-and-pepper pattern

(Figures 5C and 5F). By E10.5, however, NKX2-1-positive cells had begun to aggregate into larger patches, though intermixed populations could still be observed, especially in the more rostral airway (Figures 5D and 5G). By E11.5, NKX2-1-expressing cells were observed predominantly in large patches that evaginated from the foregut endoderm (Figures 5E and 5H). The extent of evagination of NKX2-1 regions was variable between different NKX2-1-positive cell groups, resulting in variable patterns of dysmorphology in different *NKX2-1*$^{lox/lox}$; *Foxa2*$^{CreER/+}$ mutant foreguts (Figures 5H, 5I, and 5M). At the level of the lung bud, mosaic expression of NKX2-1 disrupted the pattern of branching morphogenesis, wherein only NKX2-1-positive regions formed lung buds. Within the rostral foregut, however, we observed protrusions undergoing a caudal-to-rostral (TE-like) separation (Figures 5I and 5I'). We observed a similar phenotype in *NKX2-1*$^{lox/lox}$; *Nkx2–5*$^{Cre/+}$ mutant foreguts at E11.5, in which NKX2-1 is deleted from the most ventral foregut but remains unperturbed laterally along its length (Figures 5J and S6). Whereas ectopic tracheal protrusions were smaller and randomly positioned in *NKX2-1*$^{lox/lox}$; *Foxa2*$^{CreER/+}$ mutants, they reliably formed ectopically separated tubes in *NKX2-1*$^{lox/lox}$; *Nkx2–5*$^{Cre/+}$ mutants and were always positioned at the lateral aspects where Nkx2–5^{Cre} created an ectopic NKX2-1 expression boundary (Figures 5J and 5J').

To determine whether these structures are actually ectopic lung buds, we assayed SOX9 expression, which is a known marker of the branching, distal lung bud epithelium. SOX9 expression levels within ectopic protrusions of *NKX2-1*$^{lox/lox}$; *Foxa2*$^{CreER/+}$ mutant foreguts matched those of the control tracheae at comparable proximodistal position (Figures 5K–5N, cyan arrows). The lung buds of both mutant and control samples exhibited strikingly higher SOX9 expression (Figures 5K–5N, red arrowheads) compared with the wild-type trachea and mutant ectopic protrusions, leading us to conclude that rostral evaginations are not ectopic lung buds but rather are trachea-like structures.

Consistent with NKX2-1's herein-established repression of *Efnb2*, NKX2-1-positive evaginations always exhibited perfectly complementary expression with the *Efnb2*$^{H2B-GFP}$ reporter (Figures 6A–6C). Interestingly, upon compound loss of *Efnb2* in *Nkx2.1*$^{lox/lox}$; *Efnb2*$^{H2B-GFP/lox}$; *Foxa2*$^{CreER/+}$ embryos at E11.5, we observed an abrogation of ectopic tracheal separation as well as a mixing of cells between the GFP-positive and negative patches (Figures 6D–6F, arrows and outlines). This recapitulates the effect that loss of *Efnb2* has upon the normal process of TE separation and cell allocation (Figure 2B'), establishing that NKX2-1 is a direct regulator of these tissue behaviors. In order to conclusively determine whether NKX2-1 normally regulates boundary formation and tracheal cell allocation, we performed lineage tracing of ventral cells in the absence of NKX2-1 function by generating NKX2-1$^{CreER/CreER}$; ROSA26$^{Ai75/+}$ mutant embryos. Following administration of tamoxifen at E9.5, we observed substantial intermixing of *NKX2-1* lineage-positive cells into the LRIG1-expressing dorsal compartment of the unseparated foregut (Figures 6G–6R). These results suggest that, like loss of dorsal EPHRIN-B2, derepression of ventral *Efnb2* results in ventral cell misallocation into the dorsal domain of the foregut. Altogether, these data indicate that the NKX2-1 boundary organizes TE separation through EPHRIN-B2-mediated cell sorting and tissue separation.

DISCUSSION

Whereas current efforts are elucidating with exquisite detail the transcriptional regulation of fate specification during organ formation, our understanding of how these transcriptional networks couple to the physical morphogenesis of organs is minimal. Here, we demonstrate that, in addition to its critical role specifying tracheal and lung cell fates, NKX2-1 also acts to define the site of TE separation by repressing the expression of EPH-RIN-B2 to create a dorsoventral NKX2-1/EPHRIN-B2 expression boundary that properly allocates dorsoventrally patterned cells and facilitates tracheal separation (Figure 7). Thus, NKX2-1 serves as a node linking tracheal fate specification and tissue separation through its regulation of EPH/EPHRIN signaling.

Though EPH/EPHRIN signaling is well known to regulate tissue separation in the rhombomeres during hindbrain development and in the somites during mesoderm development, it also regulates tissue separation in endodermal organs, such as the intestine, liver, hepatopancreatic duct, and between the urethra and rectum (Batlle et al., 2002; Cayuso et al., 2016; Dravis et al., 2004; Niethamer and Bush, 2019; Thestrup et al., 2019). In the intestinal epithelium, EPHRIN-B1 expression in the villus apposes EPHB2/EPHB3 expression in the crypt base, and loss of EPH/EPHRIN signaling results in a misallocation of crypt base cells into the villus (Batlle et al., 2002). Notably, Wnt signaling is a known regulator both of cell fate in the crypt base and of *Ephb3* expression (Batlle et al., 2002; Mah et al., 2016), suggesting that EPH/EPHRIN signaling could connect cell identity with position in this context as well. EPHRIN-B2 loss of function also results in urorectal fistula, in which the rectum is aberrantly connected to the urethra (Dravis et al., 2004; Lewis et al., 2015). The hindgut endoderm gives rise to the embryonic cloaca, which undergoes septation to form the urogenital and anorectal sinuses; EPHRIN-B2 expression is enriched within the ventral aspect of the hindgut endoderm that gives rise to the urogenital sinus but is not detected in the dorsal hindgut endoderm that gives rise to the anorectal sinus (Dravis et al., 2004). Though the developmental function of EPHRIN-B2 in this context remains unknown, it is tempting to speculate that it may organize the site of urorectal septation in a manner that mirrors its role in TE separation.

EPHRIN-B2 reverse signaling has been previously implicated in TEF, hindgut malformations, and defects in secondary palate fusion using an $Efnb2^{lacZ}$ mutation in which the intracellular domain has been replaced with lacZ (Dravis et al., 2004). $Ephb2^{-/-}$; $Ephb3^{-/-}$ compound mutants display some similar phenotypes that are also observed in trans-heterozygous $Efnb2^{lacZ/+}$; $EphB2^{+/-}$; $EphB3^{+/-}$ compound mutants, indicating genetic interaction between *Efnb2* and *Ephb2/b3* in these contexts (Dravis and Henkemeyer, 2011; Dravis et al., 2004). However, due to the documented hyperactivation of EPH receptor forward signaling by the $Efnb2^{lacZ}$ mutant employed in these studies (Zhang et al., 2015), it remains unclear whether these phenotypes are consequences of loss of function of EPHRIN-B2 reverse signaling or gain of function of EPH receptor activation. Indeed, our own interrogation using a separate *Efnb2* loss-of-function model could not confirm that palate phenotypes are attributable to EPHRIN-B2 loss of function (Lewis et al., 2015). Further, whereas we and others recover $Efnb2^{H2BGFP/+}$ heterozygotes at expected ratios (Davy and Soriano, 2007), $Efnb2^{lacZ/+}$ heterozygous mutants sometimes exhibited cleft

palate, further supporting a gain-of-function mode of action of this allele, at least in some contexts. Based on multiple lines of evidence presented here and previously (Dravis and Henkemeyer, 2011; Lewis et al., 2015), failed TE separation and hindgut malformations are the consequences of EPHRIN-B2 loss of function, and it is therefore possible that these are bona fide contexts that require reverse signaling, but further study will be needed to disentangle these mechanisms definitively. The above results speak to the complexity of the EPH/EPHRIN signaling system and to the challenges inherent to dissecting forward and reverse signaling functions *in vivo* (Niethamer and Bush, 2019).

Recent studies have posited the importance of the dorsoventral boundary MECs, which express both NKX2-1 and SOX2 and which we find are ventrally adjacent to the EPHRIN-B2-expressing cells of the dorsal foregut (Kim et al., 2019; Nasr et al., 2019). Our data help to explain the significance of the MECs, indicating that NKX2-1 represses EPHRIN-B2 to generate a dorsoventral expression differential that defines the site of TE separation. We find, however, that an EPHRIN-B2 boundary is not sufficient to drive separation morphogenesis in the absence of NKX2-1, indicating that other targets of NKX2-1 are also required. *Epha4*, *Epha7*, and *Efna1* were all identified as targets of NKX2-1 regulation in our recent RNA-seq study of TE morphogenesis (Figure S7A; Kuwahara et al., 2020). Expression analysis of these and other EPH/EPHRINS in *NKX2-1* mutants compared with controls corroborates that *Efna1* and *Epha4* are enriched in tracheal-fated endoderm (Figures S7B–S7I’); that *Efna1*, *Epha4*, and *Epha7* are downregulated upon loss of *NKX2-1* (Figures S7B–S7M’); and that *Ephb2*, *Ephb3*, and *Ephb4* remain unperturbed upon loss of *NKX2-1* (Figures S7N–S7Y’). These discoveries imply that a broader morphogenetic program driven by EPH/EPHRIN segregation likely lies downstream of NKX2-1 and contributes to foregut development. Though SOX2 was not required for *Efnb2* expression within the dorsal foregut, its expression at NKX2-1/EPHRIN-B2 boundaries was required for ectopic tissue separation. Further, loss of SOX2 from the ventral foregut, including the MEC boundary population, also resulted in loss of TE separation. This function was presumably not only to repress NKX2-1, as an NKX2-1 boundary still existed in these embryos. These data suggest that SOX2 may regulate key targets that work together with the NKX2-1/EPHRIN-B2 program to organize TE separation. Because SOX2 is not restricted to only dorsal esophageal cell types but is also expressed in MECs (Figures S1F), we cannot determine whether these targets are within the MECs, within the dorsal NKX2-1-negative cells, or on both sides of the NKX2-1/EPHRIN-B2 boundary; investigation of the transcriptional networks downstream of SOX2 will help to clarify this question.

Though we show here that EPHRIN-B2 is required within the foregut endoderm for TE separation, the tissues in which partner EPH receptors function are not clear. We observe that multiple receptors for EPHRIN-B2 are expressed within both the foregut endoderm and the surrounding mesenchyme, suggesting two non-exclusive possibilities. First, EPH receptor enrichment within the lateral splanchnic mesenchyme suggests the possibility that endodermal EPHRIN-B2 signals to the lateral mesenchyme to contribute to medial constriction that has been proposed to initiate foregut separation (Nasr et al., 2019). Consistent with this, we find that *Efnb2* mutant foreguts do not exhibit any apparent medial constriction. In EPHRIN-B2-dependent ectopic trachea-like separation in *NKX2-1* mosaic mutant embryos, these ectopic boundaries would organize mesenchymal

constriction at aberrant sites, possibly through signaling of EPHRIN-B2 from the endoderm to the adjacent mesenchyme. Second, based on the patterns of expression we observe, signaling between EPHRIN-B2 and EPH receptors within the foregut endoderm may drive repulsive segregation at the NKX2-1/EPHRIN-B2 boundary, resulting in the proper allocation of tracheal cells, a possibility that is further supported by our analysis of foregut EPH receptor phosphorylation. Unlike in the zebrafish hindbrain rhombomeres, which exhibit complementary patterns of EPHRIN and EPH expression, the murine foregut endoderm exhibits differential expression only of EPHRIN-B2 without stark complementary expression of EPH receptor expression. This situation is similar to our observations of Efnb1$^{+/-}$ mutant embryos, in which mosaic expression of *Efnb1* leads to cell segregation of EPHRIN-B1-positive and negative cells despite uniform EPHB receptor expression (Bush and Soriano, 2010; Niethamer et al., 2020). It is also possible that signaling within the endoderm regulates adhesion of MECs during a process of septal fusion to separate the trachea and esophagus. Similar roles for EPH/EPHRIN signaling in tissue fusion have been previously proposed in neural tube closure, urorectal development, and secondary palate fusion (Dravis and Henkemeyer, 2011; Holmberg et al., 2000). Though we did not observe disruption of TE separation upon endodermal loss of a preferred receptor, EPHB4, it is possible that it works redundantly with other receptors. Future work will be required to disentangle the tissue-specific function of distinct receptors in TE separation morphogenesis.

The downstream cellular mechanisms by which EPH/EPHRIN signaling regulates boundary formation in this context likely include cell repulsion, which has been repeatedly demonstrated to mediate EPH/EPHRIN cell-sorting behaviors in a wide variety of contexts (Canty et al., 2017; Kindberg et al., 2021; O'Neill et al., 2016; Poliakov et al., 2008; Taylor et al., 2017; Xu et al., 1995, 1999). Recent work supports a model of EPH/EPHRIN segregation in which EPH- and EPHRIN-expressing cells sort and separate from one another through impacts on the strength of cell contacts by modulation of the actin cytoskeleton (Canty et al., 2017; Kindberg et al., 2021). Notably, in our recent work, cellular aggregates that had undergone EPH/EPHRIN-mediated segregation further underwent a form of partial or complete tissue separation that is highly similar to the sorting behavior and tissue separation phenotypes we observe in *NKX2-1* mosaic mutant embryos. Though additional work will be needed to define the precise cellular mechanisms by which cell sorting occurs in TE separation, our results are consistent with the role of EPH/EPHRIN signaling in boundary formation and demonstrate how a cell fate program and morphogenetic program are coupled to facilitate organogenesis.

Limitations of the study

We have demonstrated that NKX2-1 regulates *Efnb2* genetically and binds at multiple sites near the *Efnb2* gene, but detailed interrogation of the mechanism of regulation remains to be performed. To functionally validate NKX2-1-binding sites, we performed luciferase reporter experiments in an immortalized cell line. Though these experiments consistently show that identified NKX2-1-binding sites are functionally relevant silencers, the requirement of canonical consensus NKX2-1-binding sequences is not completely consistent, possibly suggesting a more nuanced situation or reflecting the limitations of the use of this exogenous enhancer and promoter assay. Future studies will therefore include *in vivo* functional

interrogation of putative suppressor sequences. We additionally note that, despite the experiments described herein, the EPH-receptor-signaling partners of EPHRIN-B2 in this context remain unknown. While it is conceivable that a receptor-independent mode of activity may be employed, we feel that additional compound genetic analysis is indicated. Remedying these shortcomings forms the basis for continuing experimentation in the lab.

STAR★METHODS

RESOURCE AVAILABILITY

Lead contact—Further information and requests for resources and reagents should be directed to and will be fulfilled by the lead contact, Jeffrey Bush (jeffrey.bush@ucsf.edu).

Materials availability—Luciferase reporter constructs generated for this manuscript can be made available upon request.

Data and code availability

- Sequencing datasets analyzed here were originally published and made available in Kuwahara et al. (2020). All other data reported in this paper will be shared by the lead contact upon request.
- This paper does not report original code.
- Any additional information required to reanalyze the data reported in this paper will be made available from the lead contact upon request.

EXPERIMENTAL MODEL AND SUBJECT DETAILS

Mice—The following preexistent mouse alleles were used in this study: *Efnb2*^{CR} (MGI#5882571), *Efnb2*$^{H2B\text{-}GFP}$ (MGI#3526818), *Efnb2*^{lox} (MGI#2176538), *Ephb4*^{lox} (MGI#5575404), *Foxa2*^{CreER} (MGI#3774420), *Gata4-G4-Cre*^{Tg} (MGI#4840244), *NKX2-1*^{CreER} (MGI#5302534), *NKX2-1*^{lox} (MGI#3653645), *Nkx2–5*$^{IRES\text{-}Cre}$ (MGI#2448972), *ROSA26*^{Ai75} (MGI#5603432), *ROSA26*^{lacZ} (MGI#1861932), *ROSA26*^{mTmG} (MGI#3716464), *Shh*$^{Cre\text{-}EGFP}$ (MGI#3053959), *Sox2*^{CreER} (MGI#5295990), *Sox2*^{lox} (MGI#4366453), *Tie2-Cre*^{Tg} (MGI#3608912). The *NKX2-1*$^{-}$ allele was produced by germline recombination of the *NKX2-1*^{lox} allele, referenced above.

Numbers of samples represented in all figure panels are reported in Table S1. All samples are of embryonic staging, also reported in Table S1, for which gender has not been determined.

All animal procedures were performed at the University of California at San Francisco (UCSF) under approval from the UCSF Institutional Animal Care and Use Committee (mouse protocol # AN164190).

METHOD DETAILS

Injections—Batches of tamoxifen solution were prepared by sonication of 20 mg/mL tamoxifen (Sigma, T5648), 5% (vol/vol) EtOH, and 95% (vol/vol) sunflower seed oil

(Sigma, S5007), used for up to 5 days, and stored at +4°C shielded from light. Pregnant dams were weighed and injected intraperitoneally at the specified stages with 0.1 mg tamoxifen per 1 g of dam mass. BrdU solution was prepared by dissolution of 5 mg/mL of BrdU (Sigma, B5002) in 0.9% NaCl (wt/vol), which was frozen in aliquots at −20°C. Pregnant dams were weighed and injected intraperitoneally with 50 μg BrdU per 1g dam mass at the specified amount of time prior to sacrifice and embryo collection.

Histology—E15.5 embryos were processed whole, while E18.5 embryos were skinned and trisected to capture the region below the mandible and above the abdomen. Samples were fixed in Bouin's fixative (Sigma, HT101128) at room temperature and graded into EtOH, histoclear (National Diagnostics, HS-200), and paraffin before being embedded in paraffin. Coronal serial sections were cut at a thickness of 7 μm and subsequently stained with hematoxylin and eosin. Imaging was performed on a Zeiss Imager.Z2 and 3D reconstructed models were produced using Avizo (ThermoFisher): sections were aligned using the "align slices" function, lumens of the pharynx, larynx, trachea, bronchi, and esophagus model labels were selected by thresholding for unstained regions and selecting with the "magic wand" tool within the segmentation pane, model labels were processed using the "resample" tool with "voxel averaging" of "3 × 3 × 1", a surface model was generating using "generate surface" with "constrained smoothing" of "extent" 2, and models were visualized with the "surface view" module.

Section immunofluorescence and RNAScope—All stages of embryo were processed whole, with the exception that E18.5 embryos were skinned and trisected to capture the region below the maxilla and above the abdomen. Samples were fixed in 4% paraformaldehyde (wt/vol) in PBS, graded to 30% sucrose (wt/vol) in PBS, embedded in OCT (TissueTek, 4583), and stored at −80°C. Sections were cut at a thickness of 10 μm and stored with desiccant at −20°C. RNAScope was performed using the "Fluorescent Multiplex V2" assay and with probes hybridizing to *Efna1* (428621), *Epha4* (419081), *Epha7* (430961-C2), *Ephb2* (447611), *Ephb3* (510251), and *Ephb4* (498201). Immunofluorescence was performed according to standard techniques with antibodies against acetylated α-tubulin (1:250, Sigma, T7451), BrdU (1:150, Abcam, ab6326), cleaved caspase3 (1:200, Cell Signaling, 9661), EPHA4 (1:75, R&D, AF641), EPHB2 (1:75, R&D, AF467), EPHB3 (1:75, R&D, AF432), EPHB4 (1:75, R&D, AF446), phospho-EPHA2+A3+A4 (1:150, Abcam, ab62256), phospho-EPHB1+B2 (1:150, Abcam, ab61791), GFP (1:500, Abcam, ab13970), KRT5 (1:250, BioLegend, 905501), KRT8 (1:75, DSHB, AB_531826), LRIG1 (1:200, R&D, AF3688), MUC5B (1:300, Santa Cruz Biotechnology, sc-20119), NKX2-1 (1:150, Millipore, 07–601), NKX2-1 (1:100, Santa Cruz Biotechnology, sc-8761), NKX2-1 (1:300, ThermoFisher, MS-699), RFP (1:250, Abcam, ab62341), SOX2 (1:300, Neuromics, GT15098), and SOX2 (1:250, Seven Hills Bioreagents, WRAB-1236). Staining for BrdU required antigen retrieval by incubating sections in 2N HCl at 37°C for 10 min. Staining for cleaved caspase3 and NKX2-1 (Millipore, 07–601) required antigen retrieval by incubating sections at 100°C in 10 mM NaCitrate, pH6, for 20 min. Staining for phosphorylated EPH receptors required the use of TBS in place of PBS at every step of the process, beginning with the isolation of embryos. Imaging was performed on a Zeiss Imager.Z2, a Zeiss LSM900, or a Leica SP8.

Whole-mount immunofluorescence—E9.5 embryos were processed whole, while E10.5 and E11.5 embryonic foreguts were isolated for tissue processing. Samples were fixed in 4% paraformaldehyde (wt/vol) in PBS, graded into MeOH, and stored at −20°C. Whole-mount immunofluorescence was performed according to standard protocols with antibodies against e-cadherin (1:300, Invitrogen, 13–1900), NKX2-1 (1:300, ThermoFisher, MS-699), SOX2 (1:300, Neuromics, GT15098), and SOX9 (1:200, R&D Systems, AF3075). Stained samples were then graded through MeOH into a clearing solution of 1:2 Benzyl Alcohol:Benzyl Benzoate, and imaging was performed on a Zeiss LSM900, a Zeiss LSM880, or a Leica SP8. 3D renderings of foregut endoderm were generated using the software Avizo (ThermoFisher): Z stacks were resampled along the rostro-caudal axis to simplify segmentation using the "resample" function, segmentation was performed on the "segmentation" pane using the "magic wand" tool by thresholding immunostaining for E-Cadherin to select endodermal tissue in intervals of optical slices, "interpolation" was performed to fill in endodermal selection between these slices, the resulting selection was inspected visually to ensure that only endodermal tissue was selected, mesenchymal staining was removed from the 3D renderings using the "arithmetic" function in order to more clearly visualize endodermal staining, renderings were visualized using the "volume rendering" function at "high quality" and with no "lighting" effects.

ChIP-seq and ChIP-qPCR—ChIP-seq data were previously generated (Kuwahara et al., 2020), and identification of candidate NKX2-1 regulatory regions near *Efnb2* was performed visually using Integrative Genomics Viewer (Robinson et al., 2011). ChIP for NKX2-1 in E11.5 foreguts was performed as described (Kuwahara et al., 2020). qPCR for candidate NKX2-1 binding regions was performed using iTaq Universal Sybr Green Supermix (BioRad 1725125) in 10 μL reactions consisting of 5 μL Sybr mix, 2 μL Nkx2.1 immunoprecipitate, IgG immunoprecipitate, or 1:100 input DNA, and 0.5 μL primers. Reactions were run in triplicate for each of two biological replicates on a BioRad CFX96 qPCR machine. Negative control primers: 5′-CAA-GGC-TTC-GTG-ACC-AGG-AAG-3′ and 5′-GG-AAC-AGA-AGTGAG-CTA-AGA-CCA-C-3′, SR+845 primers: 5′-GAG-TGT-GGA-CTC-AGG-AAG-CAC-3′ and 5′-GAG-CCC-CTT-ATG-TCA-ACTCAC-AG-3′, SR+646 primers: 5′-GTC-ACT-CTG-GCT-TGA-TGC-ATA-G-3′ and 5′-CTA-CGG-CTG-CTG-GGA-GTG-TG-3′, SR+130 primers: 5′-CCA-TTA-GAG-TGT-TCC-AAA-TGG-G-3′ and 5′-CGG-TGC-TTG-GAT-TTC-TTC-TC-3′, SR-1920 primers: 5′-CCA-AAC-CCA-ATA-CTC-AAT-CAA-G-3′ and 5′-CTT-CTG-CTT-TTC-CAC-TTG-CAT-C-3'.

Reporter construct design—Reporter plasmids were constructed using pNL1.1.PGK[*Nluc*/PGK] (Promega, N1441) and pNL1.1.TK[*Nluc*/TK] (Promega, N1501) plasmids; these plasmids contain PGK or TK constitutively active promoters, selected to assure a basal level of transcriptional activity. Candidate silencer regions (SRs) were inserted by restriction fragment ligation upstream of the promoters between unique *SfiI* and *KpnI* sites. Candidate SRs were identified by ChIP-seq (Figure 4Q), and SRs – 1920, −4, +130, +646, and +845 were selected for this analysis. DNA sequences were ordered (Genewiz, PriorityGENE service) to contain: mouse genomic sequence (mm10) corresponding to the union of each significantly called peak across 2 ChIP-seq replicates flanked by 100 bp of

additional genomic sequence in both the 5′ and 3′ directions, flanked by restriction sites for constructing reporters with all elements inserted in tandem, and again flanked by *SfiI* and *KpnI* sites for insertion into the reporter plasmids. Two sets of sequences were ordered: one with wildtype sequence, and one in which NKX2-1 consensus binding sites were mutated by base-pair substitution to adenines or thymines. After inserting each wildtype and mutated individual and in-tandem sequence into both reporter plasmids, the resulting reporter constructs were tested by sequencing (Genewiz, Sanger Sequencing service) to verify the correct insertions were made.

Cell culture and luciferase assays—MLE-15 cells were cultured in DMEM +10% FBS + l-glut + P/S. For the luciferase assay, a dual-luciferase assay reporter system (Promega, N1610) was selected, in which pGL4.53[*luc2*/PGK] and pGL4.54[*luc2*/TK] plasmids were co-transfected with the corresponding experimental plasmids to normalize for differing transfection efficiency and cell number. Transient transfection was performed using Lipofectamine 2000 reagent (Thermo, 11668027) according to the manufacturer's protocol, substituting DMEM for Opti-MEM medium, in 96-well opaque walled plates. Lipofectamine/DNA complexes were prepared in triplicate for each reporter and control construct, using 2μL of lipofectamine per well and a 10:1 ratio of experimental:normalizing plasmid totaling 100 ng per well, and placed into the plate along with ~60μL of culture medium without antibiotics. Cells were suspended in culture medium without antibiotics at a density of ~1.7 M/mL, and ~30μL (~50K cells) were added to each well. After 6 h of culture, media was replaced with antibiotic-containing media. Luminescence assay was performed according to the manufacturer's protocol after 24 h of culture on a BioTek Synergy 2 plate reader. Transfections were performed in triplicate for each condition on a single plate, and this experiment was performed three times.

QUANTIFICATION AND STATISTICAL ANALYSIS

Cell proliferation and apoptosis—Sections were assigned to rostral, middle, or caudal bins of the foregut, comprising equal thirds ranging from the pharynx to the bifurcation of the lung buds. Proliferation score was determined for each section as the percentage of BrdU-positive endodermal cells out of the total number of endodermal cells. Apoptosis score was determined for each section as follows: images of cleaved caspase3 stains were collected under identical imaging conditions, the endoderm was digitally isolated, cleaved caspase3 stain was thresholded identically across all sections, and scores were assigned as a percentage of pixels positive for cleaved caspase3-positive out of total pixels. Control scores were pooled, as were mutant scores, and a two-tailed Welch's T test was performed to test the hypothesis that no significant difference existed between mutant and control for proliferation or apoptosis scores, for which a cutoff of $p = 0.05$ was used to determine significance.

ChIP-qPCR—Percentage input was calculated as follows: AdjInput=(mean input Ct)-6.644, %input = 100*2^[(AdjInput)-(mean IP Ct)]. Standard deviation of mean percentage input was calculated as follows: stdev(input - IP) = SQRT[(Input stdev^2)+ (NKX2.1 IP stdev^2)]. Upper error = [100*2^((adjInput - IP) + stdev(input - IP)] - %input, Lower error = %input - [100*2^((adjInput - IP) - stdev(input - IP)]. Statistical significance

of the NKX2-1 ChIP versus IgG was determined with a student's T test using p = 0.05 as a cutoff for significance.

Luciferase luminescence—Normalized luminescence was calculated by dividing the NanoLuciferase raw score by the FireflyLuciferase raw score. The resulting scores were presented as a percentage of the mean of the positive control. Means were calculated for each experimental and control condition across three experiments. Statistical significance was determined comparing each experimental reporter with the positive control and comparing each mutated reporter with its corresponding wildtype reporter by a two-tailed pairwise T test using a significance cutoff of p = 0.05.

Supplementary Material

Refer to Web version on PubMed Central for supplementary material.

ACKNOWLEDGMENTS

We thank the labs of Jeffrey Whitsett and Michael Beers for providing MLE-15 cells. We are grateful for outstanding mouse colony genotyping support from Fang-Shiuan Leung. We thank Terren Niethamer, Julie Sneddon, Ralph Marcucio, Marisol O'Neill, and Abby Kindberg for critical reading and constructive feedback on the manuscript. This work was supported by R01HL144785 from NIH/NHLBI to J.O.B. A.K. was supported by GRFP1650113 from NSF.

REFERENCES

Arnold K, Sarkar A, Yram MA, Polo JM, Bronson R, Sengupta S, Seandel M, Geijsen N, and Hochedlinger K (2011). Sox2(+) adult stem and progenitor cells are important for tissue regeneration and survival of mice. Cell stem cell 9, 317–329. [PubMed: 21982232]

Batlle E, Henderson JT, Beghtel H, van den Born MM, Sancho E, Huls G, Meeldijk J, Robertson J, van de Wetering M, Pawson T, et al. (2002). Beta-catenin and TCF mediate cell positioning in the intestinal epithelium by controlling the expression of EphB/ephrinB. Cell 111, 251–263. [PubMed: 12408869]

Billmyre KK, Hutson M, and Klingensmith J (2015). One shall become two: separation of the esophagus and trachea from the common foregut tube. Dev. Dyn. 244, 277–288. [PubMed: 25329576]

Braren R, Hu H, Kim YH, Beggs HE, Reichardt LF, and Wang R (2006). Endothelial FAK is essential for vascular network stability, cell survival, and lamellipodial formation. J. Cell Biol. 172, 151–162. [PubMed: 16391003]

Bruno MD, Bohinski RJ, Huelsman KM, Whitsett JA, and Korfhagen TR (1995). Lung cell-specific expression of the murine surfactant protein A (SP-A) gene is mediated by interactions between the SP-A promoter and thyroid transcription factor-1. J. Biol. Chem. 270, 6531–6536. [PubMed: 7896788]

Bush JO, and Soriano P (2010). Ephrin-B1 forward signaling regulates craniofacial morphogenesis by controlling cell proliferation across Eph-ephrin boundaries. Genes Dev. 24, 2068–2080. [PubMed: 20844017]

Canty L, Zarour E, Kashkooli L, Franç ois P, and Fagotto F (2017). Sorting at embryonic boundaries requires high heterotypic interfacial tension. Nat. Commun. 8, 157. [PubMed: 28761157]

Cayuso J, Xu Q, and Wilkinson DG (2015). Mechanisms of boundary formation by Eph receptor and ephrin signaling. Dev. Biol. 401, 122–131. [PubMed: 25448699]

Cayuso J, Dzementsei A, Fischer JC, Karemore G, Caviglia S, Bartholdson J, Wright GJ, and Ober EA (2016). EphrinB1/EphB3b coordinate bidirectional epithelial-mesenchymal interactions controlling liver morphogenesis and laterality. Dev. Cell 39, 316–328. [PubMed: 27825440]

Choe CP, and Crump JG (2015). Eph-Pak2a signaling regulates branching of the pharyngeal endoderm by inhibiting late-stage epithelial dynamics. Development 142, 1089–1094. [PubMed: 25725065]

Chrencik JE, Brooun A, Kraus ML, Recht MI, Kolatkar AR, Han GW, Seifert JM, Widmer H, Auer M, and Kuhn P (2006). Structural and biophysical characterization of the EphB4 EphrinB2 protein-protein interaction and receptor specificity. J. Biol. Chem. 281, 28185–28192. [PubMed: 16867992]

Cooke J, Moens C, Roth L, Durbin L, Shiomi K, Brennan C, Kimmel C, Wilson S, and Holder N (2001). Eph signalling functions downstream of Val to regulate cell sorting and boundary formation in the caudal hindbrain. Development 128, 571–580. [PubMed: 11171340]

Davy A, and Soriano P (2007). Ephrin-B2 forward signaling regulates somite patterning and neural crest cell development. Dev. Biol. 304, 182–193. [PubMed: 17223098]

Domyan ET, Ferretti E, Throckmorton K, Mishina Y, Nicolis SK, and Sun X (2011). Signaling through BMP receptors promotes respiratory identity in the foregut via repression of Sox2. Development 138, 971–981. [PubMed: 21303850]

Dravis C, and Henkemeyer M (2011). Ephrin-B reverse signaling controls septation events at the embryonic midline through separate tyrosine phosphorylation-independent signaling avenues. Dev. Biol. 355, 138–151. [PubMed: 21539827]

Dravis C, Yokoyama N, Chumley MJ, Cowan CA, Silvany RE, Shay J, Baker LA, and Henkemeyer M (2004). Bidirectional signaling mediated by ephrin-B2 and EphB2 controls urorectal development. Dev. Biol. 271, 272–290. [PubMed: 15223334]

Gerety SS, Wang HU, Chen ZF, and Anderson DJ (1999). Symmetrical mutant phenotypes of the receptor EphB4 and its specific transmembrane ligand ephrin-B2 in cardiovascular development. Mol. Cell 4, 403–414. [PubMed: 10518221]

Goss AM, Tian Y, Tsukiyama T, Cohen ED, Zhou D, Lu MM, Yamaguchi TP, and Morrisey EE (2009). Wnt2/2b and beta-catenin signaling are necessary and sufficient to specify lung progenitors in the foregut. Dev. Cell 17, 290–298. [PubMed: 19686689]

Guazzi S, Price M, De Felice M, Damante G, Mattei MG, and Di Lauro R (1990). Thyroid nuclear factor 1 (TTF-1) contains a homeodomain and displays a novel DNA binding specificity. EMBO J. 9, 3631–3639. [PubMed: 1976511]

Harfe BD, Scherz PJ, Nissim S, Tian H, McMahon AP, and Tabin CJ (2004). Evidence for an expansion-based temporal Shh gradient in specifying vertebrate digit identities. Cell 118, 517–528. [PubMed: 15315763]

Harris-Johnson KS, Domyan ET, Vezina CM, and Sun X (2009). beta-Catenin promotes respiratory progenitor identity in mouse foregut. Proc. Natl. Acad. Sci. U.S.A. 106, 16287–16292. [PubMed: 19805295]

Holmberg J, Clarke DL, and Frisén J (2000). Regulation of repulsion versus adhesion by different splice forms of an Eph receptor. Nature 408, 203–206. [PubMed: 11089974]

Ioannides AS, Massa V, Ferraro E, Cecconi F, Spitz L, Henderson DJ, and Copp AJ (2010). Foregut separation and tracheo-oesophageal malformations: the role of tracheal outgrowth, dorso-ventral patterning and programmed cell death. Dev. Biol. 337, 351–362. [PubMed: 19913007]

Jülich D, Mould AP, Koper E, and Holley SA (2009). Control of extracellular matrix assembly along tissue boundaries via Integrin and Eph/Ephrin signaling. Development 136, 2913–2921. [PubMed: 19641014]

Kania A, and Klein R (2016). Mechanisms of ephrin-Eph signalling in development, physiology and disease. Nat. Rev. Mol. Cell Biol. 17, 240–256. [PubMed: 26790531]

Kim E, Jiang M, Huang H, Zhang Y, Tjota N, Gao X, Robert J, Gilmore N, Gan L, and Que J (2019). Isl1 regulation of Nkx2.1 in the early foregut epithelium is required for trachea-esophageal separation and lung lobation. Dev. Cell 51, 675–683.e4. [PubMed: 31813798]

Kindberg AA, Srivastava V, Muncie JM, Weaver VM, Gartner ZJ, and Bush JO (2021). EPH/EPHRIN regulates cellular organization by actomyosin contractility effects on cell contacts. J. Cell Biol. 220, e202005216. [PubMed: 33798261]

Kuwahara A, Lewis AE, Coombes C, Leung F-S, Percharde M, and Bush JO (2020). Delineating the early transcriptional specification of the mammalian trachea and esophagus. Elife 9, e55526. [PubMed: 32515350]

Lewis AE, Hwa J, Wang R, Soriano P, and Bush JO (2015). Neural crest defects in ephrin-B2 mutant mice are non-autonomous and originate from defects in the vasculature. Dev. Biol. 406, 186–195. [PubMed: 26385750]

Mah AT, Yan KS, and Kuo CJ (2016). Wnt pathway regulation of intestinal stem cells. J. Physiol. 594, 4837–4847. [PubMed: 27581568]

Minoo P, Su G, Drum H, Bringas P, and Kimura S (1999). Defects in tracheoesophageal and lung morphogenesis inNkx2.1(−/−) mouse embryos. Dev. Biol. 209, 60–71. [PubMed: 10208743]

Mizuno K, Gonzalez FJ, and Kimura S (1991). Thyroid-specific enhancer-binding protein (T/EBP): cDNA cloning, functional characterization, and structural identity with thyroid transcription factor TTF-1. Mol. Cell. Biol. 11, 4927–4933. [PubMed: 1922026]

Morrisey EE, and Hogan BLM (2010). Preparing for the first breath: genetic and cellular mechanisms in lung development. Developmental Cell 18, 8–23. [PubMed: 20152174]

Nasr T, Mancini P, Rankin SA, Edwards NA, Agricola ZN, Kenny AP, Kinney JL, Daniels K, Vardanyan J, Han L, et al. (2019). Endosome-mediated epithelial remodeling downstream of hedgehog-gli is required for tracheoesophageal separation. Dev. Cell 51, 665–674.e6. [PubMed: 31813796]

Niethamer TK, and Bush JO (2019). Getting direction(s): the Eph/ephrin signaling system in cell positioning. Dev. Biol. 447, 42–57. [PubMed: 29360434]

Niethamer TK, Teng T, Franco M, Du YX, Percival CJ, and Bush JO (2020). Aberrant cell segregation in the craniofacial primordium and the emergence of facial dysmorphology in craniofrontonasal syndrome. PLoS Genet. 16, e1008300. [PubMed: 32092051]

O'Neill AK, Kindberg AA, Niethamer TK, Larson AR, Ho H-YH, Greenberg ME, and Bush JO (2016). Unidirectional Eph/ephrin signaling creates a cortical actomyosin differential to drive cell segregation. J. Cell Biol. 215, 217–229. [PubMed: 27810913]

Park EJ, Sun X, Nichol P, Saijoh Y, Martin JF, and Moon AM (2008). System for tamoxifen-inducible expression of cre-recombinase from the Foxa2 locus in mice. Dev. Dyn. 237, 447–453. [PubMed: 18161057]

Pasquale EB (2005). Eph receptor signalling casts a wide net on cell behaviour. Nat. Rev. Mol. Cell Biol. 6, 462–475. [PubMed: 15928710]

Poliakov A, Cotrina ML, Pasini A, and Wilkinson DG (2008). Regulation of EphB2 activation and cell repulsion by feedback control of the MAPK pathway. J. Cell Biol. 183, 933–947. [PubMed: 19047466]

Que J (2015). The initial establishment and epithelial morphogenesis of the esophagus: a new model of tracheal–esophageal separation and transition of simple columnar into stratified squamous epithelium in the developing esophagus. Wiley Interdiscip Rev. Dev. Biol. 4, 419–430. [PubMed: 25727889]

Que J, Okubo T, Goldenring JR, Nam K-T, Kurotani R, Morrisey EE, Taranova O, Pevny LH, and Hogan BLM (2007). Multiple dose-dependent roles for Sox2 in the patterning and differentiation of anterior foregut endoderm. Development 134, 2521. [PubMed: 17522155]

Robinson JT, Thorvaldsdóttir H, Winckler W, Guttman M, Lander ES, Getz G, and Mesirov JP (2011). Integrative genomics viewer. Nat. Biotechnol. 29, 24–26. [PubMed: 21221095]

Sandberg M, Flandin P, Silberberg S, Su-Feher L, Price JD, Hu JS, Kim C, Visel A, Nord AS, and Rubenstein JLR (2016). Transcriptional networks controlled by NKX2-1 in the development of forebrain GABAergic neurons. Neuron 91, 1260–1275. [PubMed: 27657450]

Sasaki T, Kusafuka T, and Okada A (2001). Analysis of the development of normal foregut and tracheoesophageal fistula in an adriamycin rat model using three-dimensional image reconstruction. Surg. Today 31, 133–139. [PubMed: 11291707]

Sher ZA, and Liu KJ (2016). Congenital tracheal defects: embryonic development and animal models. Genetics 3, 60–73.

Taylor HB, Khuong A, Wu Z, Xu Q, Morley R, Gregory L, Poliakov A, Taylor WR, and Wilkinson DG (2017). Cell segregation and border sharpening by Eph receptor-ephrin-mediated heterotypic repulsion. J. R. Soc. Interf. 14, 20170338.

Thestrup MI, Caviglia S, Cayuso J, Heyne RLS, Ahmad R, Hofmeister W, Satriano L, Wilkinson DG, Andersen JB, and Ober EA (2019). A morphogenetic EphB/EphrinB code controls hepatopancreatic duct formation. Nat. Commun. 10, 5220. [PubMed: 31745086]

Wang HU, Chen ZF, and Anderson DJ (1998). Molecular distinction and angiogenic interaction between embryonic arteries and veins revealed by ephrin-B2 and its receptor Eph-B4. Cell 93, 741–753. [PubMed: 9630219]

Wikenheiser KA, Vorbroker DK, Rice WR, Clark JC, Bachurski CJ, Oie HK, and Whitsett JA (1993). Production of immortalized distal respiratory epithelial cell lines from surfactant protein C/simian virus 40 large tumor antigen transgenic mice. Proc. Natl. Acad. Sci. U S A. 90, 11029–11033. [PubMed: 8248207]

Xu Q, Alldus G, Holder N, and Wilkinson DG (1995). Expression of truncated Sek-1 receptor tyrosine kinase disrupts the segmental restriction of gene expression in the xenopus and zebrafish hindbrain. Development 121, 4005–4016. [PubMed: 8575301]

Xu Q, Mellitzer G, Robinson V, and Wilkinson DG (1999). In vivo cell sorting in complementary segmental domains mediated by Eph receptors and ephrins. Nature 399, 267–271. [PubMed: 10353250]

Zaw-Tun HA (1982). The tracheo-esophageal septum–fact or fantasy? origin and development of the respiratory primordium and esophagus. Acta Anat. (Basel) 114, 1–21. [PubMed: 7148374]

Zhang G, Brady J, Liang W-C, Wu Y, Henkemeyer M, and Yan M (2015). EphB4 forward signalling regulates lymphatic valve development. Nat. Commun. 6, 6625. [PubMed: 25865237]

Highlights

- EPHRIN-B2 regulates trachea and esophagus separation, but not patterning
- Loss of EPHRIN-B2 permits aberrant intermixing of tracheal and esophageal cells
- NKX2-1 directly represses *Efnb2* to establish a dorsoventral separation boundary
- NKX2-1 regulates tracheoesophageal separation and tracheal cell allocation

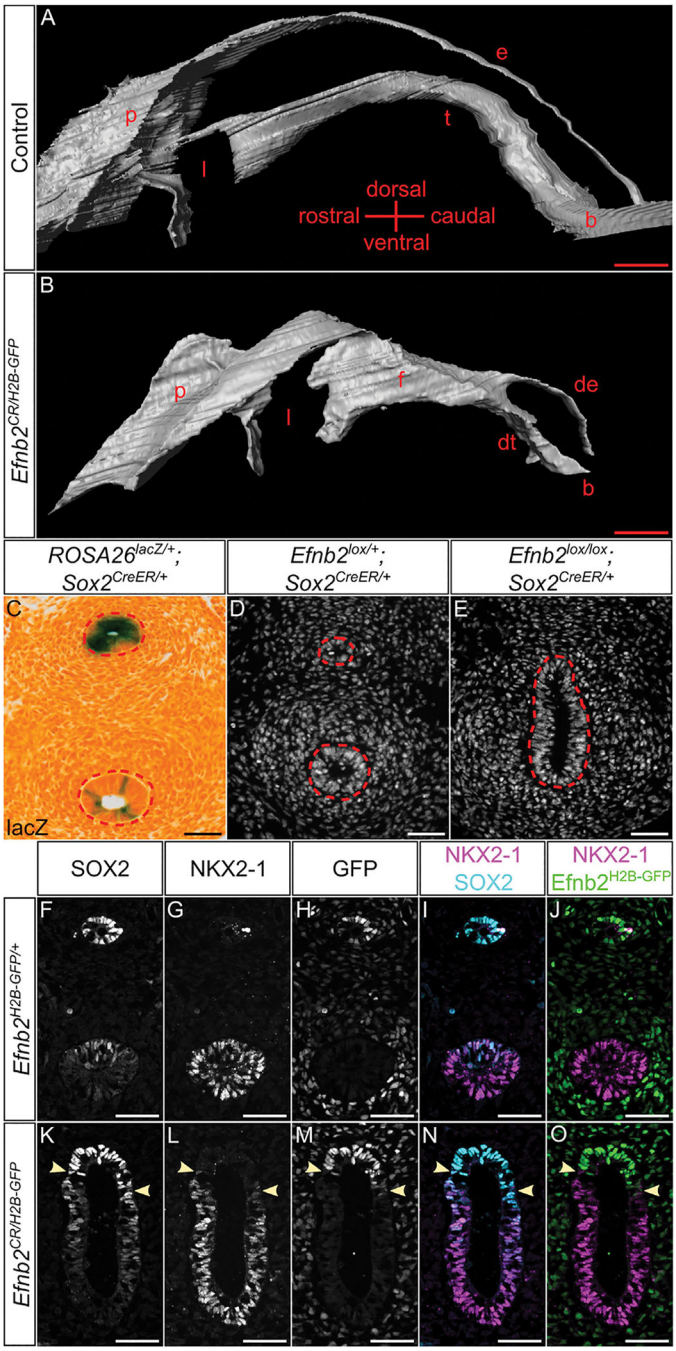

Figure 1. Endodermal EPHRIN-B2 is required for TE separation, but its loss does not disrupt dorsoventral patterning of the foregut

(A and B) 3D models of *Efnb2*$^{CR/H2B\text{-}GFP}$ mutant foregut lumens reconstructed from serial histological sections show a TEF phenotype at E15.5 (B) compared with control (A). b, bronchi; de, distal esophagus; dt, distal trachea; e, esophagus; f, fistula; l, larynx; p, pharynx; t, trachea.

(C) Lineage tracing of *Sox2*^{CreER} at E11.5 predominantly shows recombination within the esophageal epithelium following tamoxifen injections given at E7.5 and E8.5.

(D and E) DAPI stains of E11.5 foreguts reveal a failure of TE separation upon loss of endodermal EPHRIN-B2 (E) compared with *Efnb2*$^{lox/+;}$ *Sox2*$^{CreER/+}$ *trans*-heterozygote control (D). Red dotted lines outline the foregut epithelium. (F–O) Co-immunostaining of E11.5 embryos indicates that dorsoventral patterning of NKX2-1 (G and L), SOX2 (F and K), and *Efnb2* (H and M) is unperturbed by loss of EPHRIN-B2. (I, J, N, and O) Merged panels from (F), (G), (H), (K), (L), and (M) where yellow arrowheads indicate the sharp boundary between NKX2-1 (magenta) and EPHRIN-B2 reporter (green) expression, whereas SOX2 (cyan) expression extends ventrally across that boundary.
Scale bars: (A and B) 200 μm; (C–O) 50 μm.

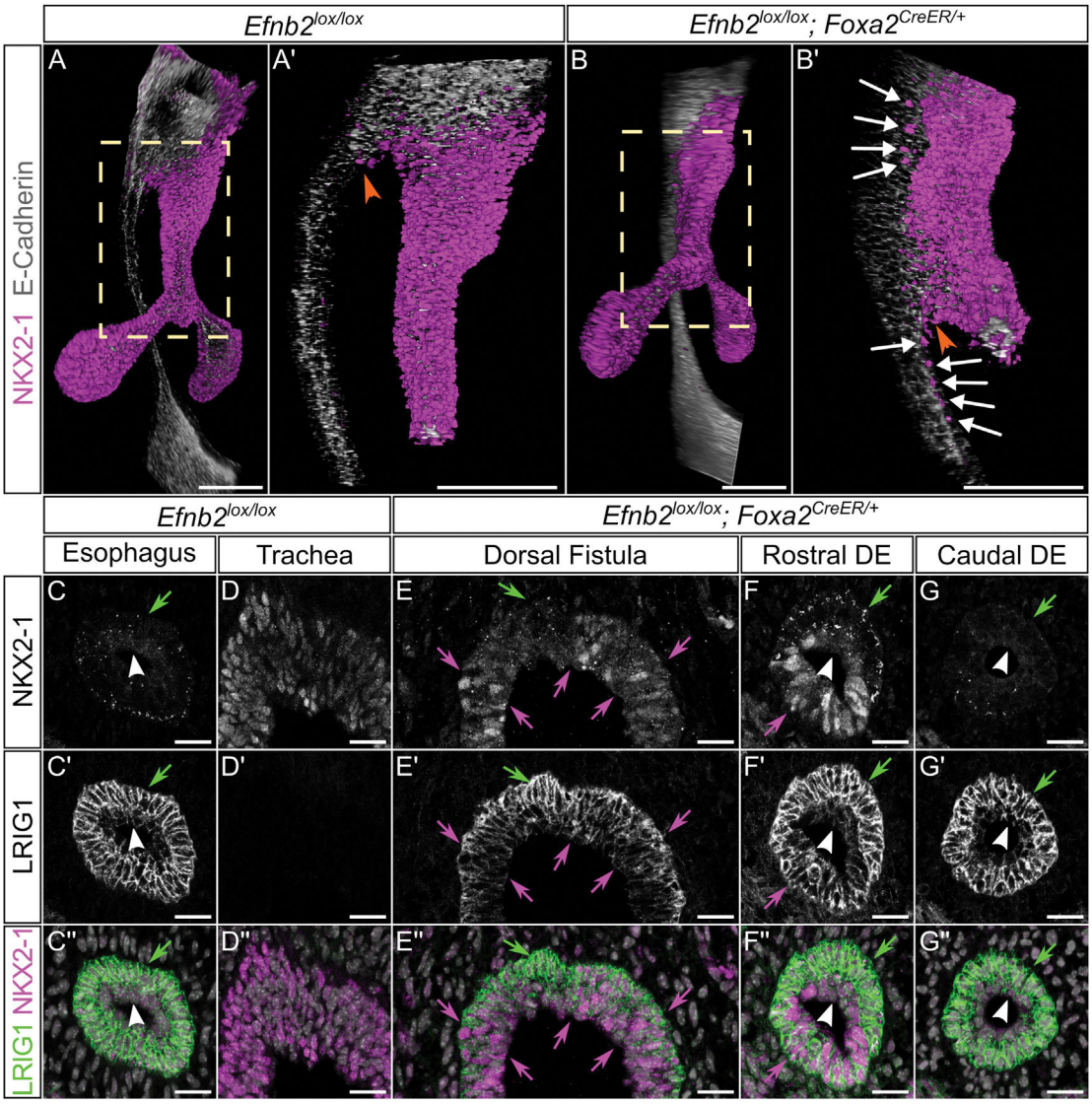

Figure 2. Loss of EPHRIN-B2 results in misallocation of NKX2-1-positive cells into the dorsal foregut and distal esophagus

(A and B) 3D renderings, segmented to visualize only epithelial signal, of confocal scans of whole-mount immunostaining of E10.5 foreguts for E-cadherin and NKX2-1 reveal failure of TE separation upon loss of EHPRIN-B2. (A' and B') High-magnification confocal scans of the approximate regions defined by dotted yellow lines in (A) and (B) and rotated slightly. Orange arrowheads indicate the dorsal aspect of the TE saddle, and white arrows indicate NKX2-1 cells intermixing dorsally across the prospective TE boundary.

(C–G") Co-immunostaining for LRIG1 (C'–G'), NKX2-1 (C–G), and their merges (C"–G") in E14.5 *Efnb2*$^{lox/lox}$*; Foxa2*$^{CreER/+}$ mutant and control embryos. Green arrows indicate basal stratified LRIG1 high-expressing cells, white arrowheads indicate apical stratified LRIG1 low-expressing cells, and magenta arrows indicate regions where infiltrating NKX2-1-positive cells have perturbed normal LRIG1 high cell position and esophageal stratification.

Scale bars: (A–B') 100 μm; (C–G") 20 μm.

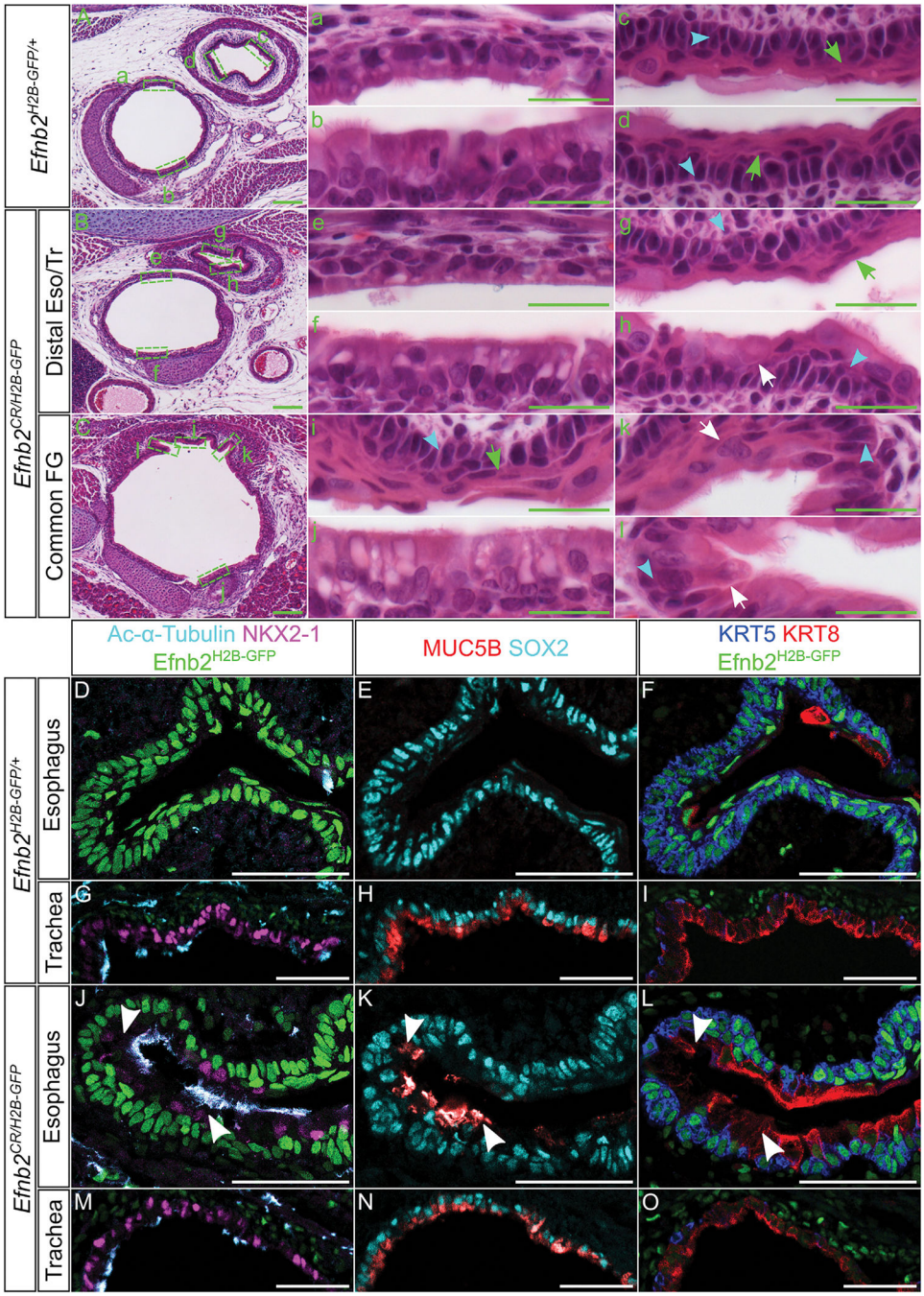

Figure 3. Misallocated NKX2-1-expressing cells give rise to tracheal cell types within the esophagus

(A–C) H&E stains of E18.5 *Efnb2*$^{CR/H2B\text{-}GFP}$ mutant embryos depicting an unseparated region of the mutant foregut (C) and a separated region (B) compared with control (A). (a–l) High-magnification images of the epithelia taken from the regions depicted in (A)–(C) by dotted green boxes are shown. Green arrows indicate apical squamous cells, cyan arrowheads indicate basal cuboidal cells, and white arrows indicate the presence of ectopic apical columnar-like cells located in the lateral regions of the unseparated foregut (i and j) and in the ventral distal esophagus (h). Scale bars: 100 μm.

(D–O) Immunostaining for markers of tracheal (NKX2-1, acetylated α-tubulin, MUC5B, and KRT8) and esophageal (SOX2 and KRT5) epithelia in the most distal, separated parts of the foregut at E18.5 in *Efnb2*$^{CR/H2B\text{-}GFP}$ mutant (J–O) and control (D–I) in adjacent sections. White arrowheads in esophageal images show the appearance of respiratory markers colocalized with NKX2-1-positive cells ectopically located with in the distal esophagus upon loss of EPHRIN-B2 (J–L),while dorsal, distal tracheal images do not reveal a detectable change in tracheal or esophageal markers in *Efnb2*$^{CR/H2B\text{-}GFP}$ mutant (M–O) compared with control trachea (GI). Scale bars: 50 μm.

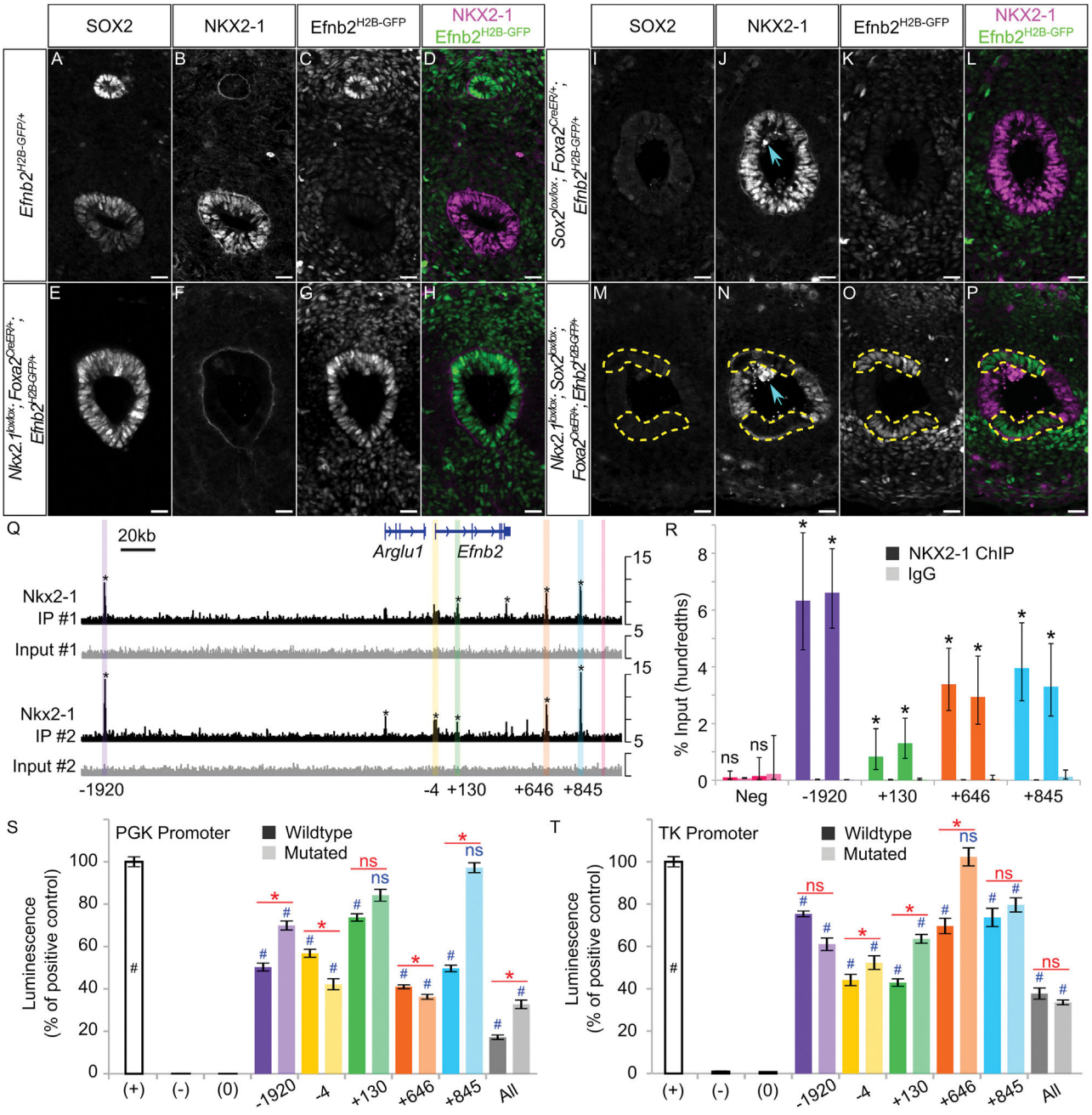

Figure 4. The *Efnb2* expression boundary is created by NKX2-1-mediated repression in the ventral endoderm

(A–P) Co-immunostaining for NKX2-1 (B, F, J, N), SOX2 (A, E, I, M), H2B-GFP (C, G, K, O), and their merges (D, H, L, P) representing *Efnb2* patterning in the specified *NKX2-1, Sox2,* and *NKX2-1; Sox2* mutants at E11.5. Loss of NKX2-1 results in de-repression of *Efnb2* GFP reporter expression, even in the absence of SOX2 (yellow dotted lines in M–P). Scale bars: 20 μm.

(Q) NKX2-1 ChIP-seq tracks show NKX2-1 binding near *Efnb2* in E11.5 foreguts across two biological replicates. NKX2-1 immunoprecipitation (IP) track is in black, input DNA track is in gray, asterisks indicate ChIP-seq peaks identified for each replicate, and regions

used in (R)–(T) are indicated by color-coded, shaded bars. Peaks are named for their approximate distance from the *Efnb2* transcription start site in hundreds of base pairs.
(R) ChIP-qPCR for NKX2-1 performed at the regions indicated in (Q) in two biological replicates. *, significantly different from corresponding IgG pull-down (negative control). Error bar calculations are defined in STAR methods.
(S and T) Luciferase assays using either a PGK (S) or TK (T) constitutively active promoter to drive luciferase expression. Controls are the reporter construct without any insertion, a similarly sized construct without the luciferase gene, and no plasmid, in order. Experimental constructs contain either individually or all in tandem DNA sequence corresponding to the peaks identified in (Q) with or without NKX2-1 consensus binding sequences mutated. Error bars represent mean ± SEM. Blue #, significantly different from promoter-only, positive control; red *, significant difference between corresponding wild-type and mutated silencers ($p < 0.05$, two-tailed paired t test).

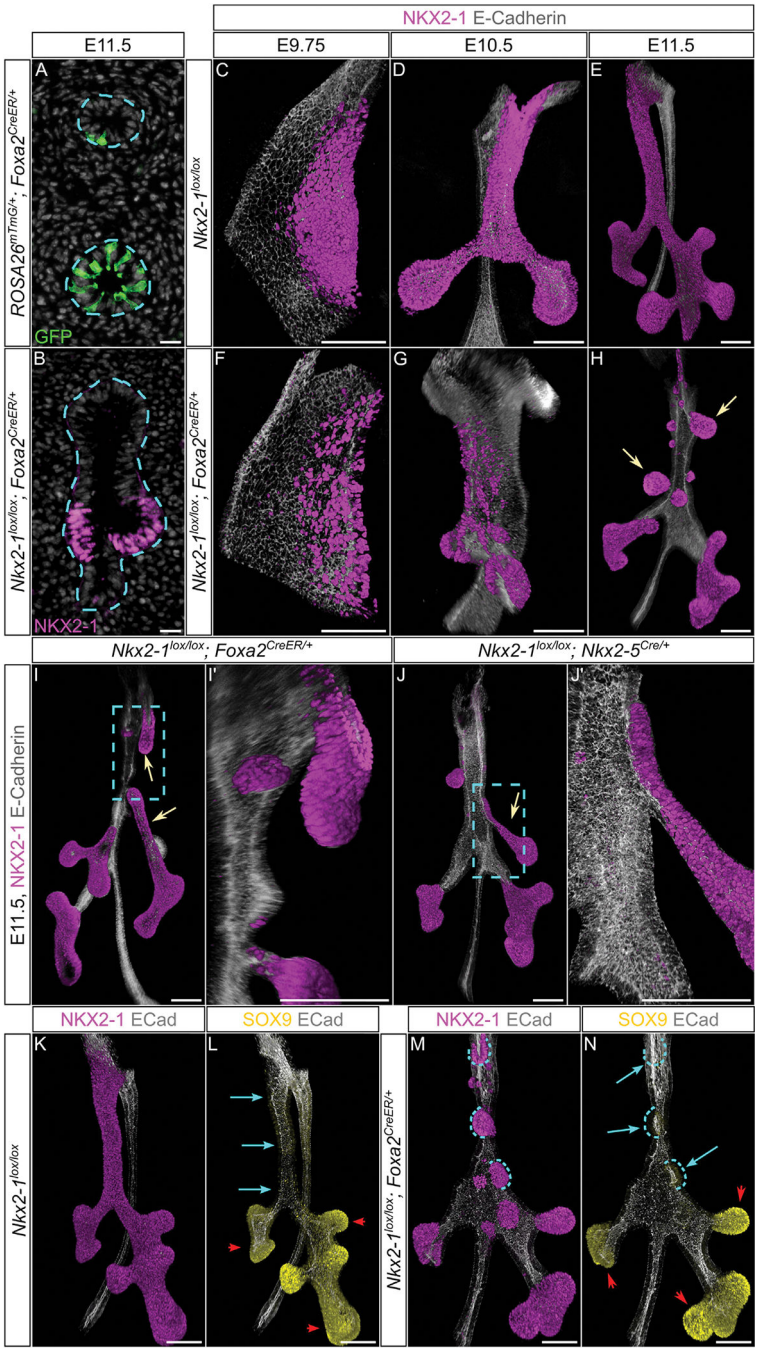

Figure 5. NKX2-1 organizes separation morphogenesis in the foregut by regulation of *Efnb2* expression

(A and B) Lineage tracing of mosaic *Foxa2*^{creER} recombination at E11.5 reveals intermixed salt-and-pepper pattern of recombined cells (A), contrasted with sorted patches of recombined cells upon mosaic loss of NKX2-1 in *NKX2-1*$^{lox/lox}$*; Foxa2*^{CreER} mutant embryos (B). Cyan dotted lines outline the foregut endoderm. (C–H) Time course imaging of *NKX2-1*$^{lox/lox}$*; Foxa2*$^{CreER/+}$ mutant and control embryos shows that NKX2-1 mosaicism begins as an intermixed, salt-and-pepper pattern at E9.75 (C and F) and resolves into sorted patches by E10.5 (D and G) and evaginate from the foregut endoderm by E11.5 (E,

yellow arrows in H). (I and J) Mosaic *NKX2-1*$^{lox/lox}$; *Foxa2*^{CreER} mutants (I) and ventral *NKX2-1*$^{lox/lox}$; *Nkx2–5*$^{Cre/+}$ mutants (J) exhibit tracheal separation at ectopic NKX2-1 expression boundaries. Yellow arrows demark ectopic tracheal separation events. (I' and J') 3D renderings of high-magnification confocal scans of the approximate regions shown by dotted cyan boxes in (I) and (J) slightly rotated highlight ectopic tracheal separation. (K–N) Co-immunostaining of E11.5 *NKX2-1*$^{lox/lox}$; *Foxa2*^{CreER} mutant and control foreguts for NKX2-1 (K and M) and SOX9 (L and N) reveals that proximal evaginations of the mutant foregut (cyan arrows and dotted lines in M and N) express levels of SOX9 consistent with proximal airway identity (cyan arrows in L), whereas more distal evaginations express higher levels of SOX9 (red arrowheads in N), consistent with control lung bud identity (red arrowheads in L). </p/. All 3D renderings are segmented to visualize only epithelial signal. Scale bars: (A and B) 20 μm, (C–N) 100 μm.

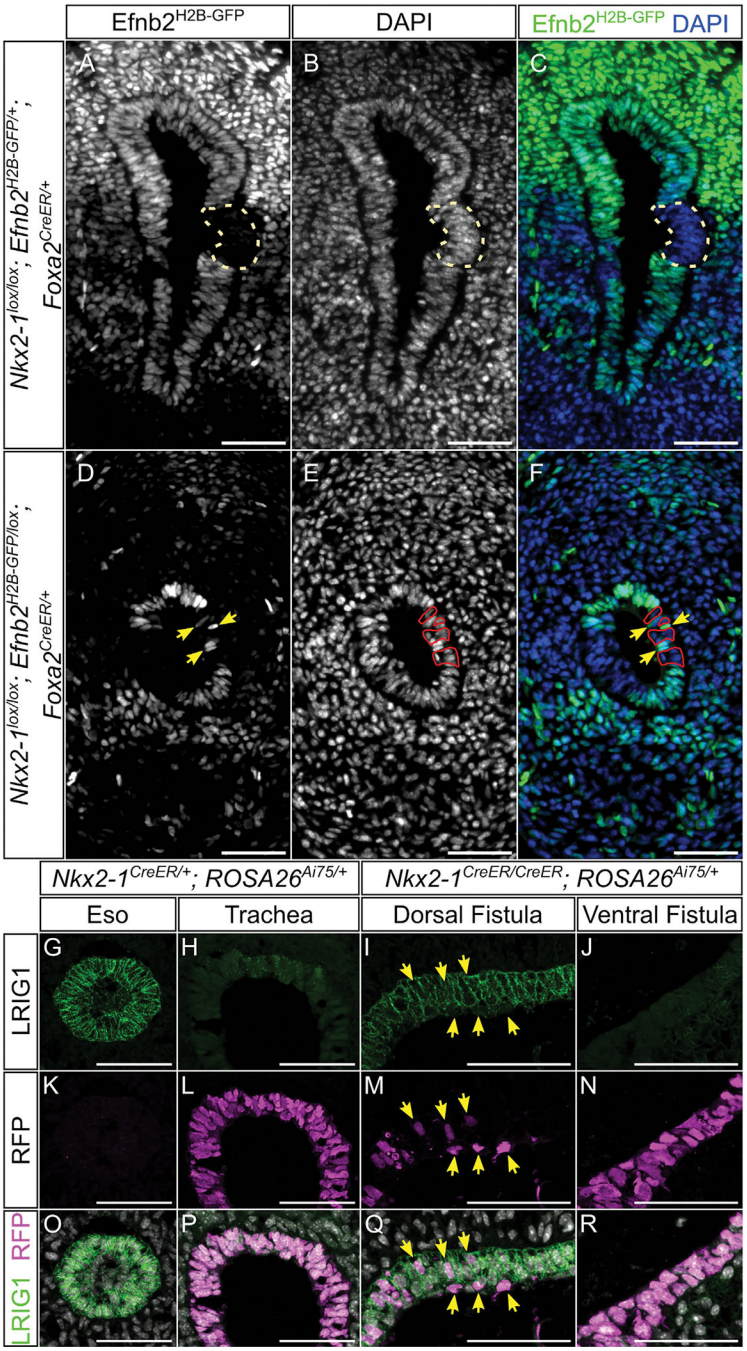

Figure 6. EHPRIN-B2 is required for NKX2-1/EPHRIN-B2 cell sorting and ectopic tracheal separation

(A–F) Immunostaining for Efnb2^{H2BGFP} reporter in mosaic *NKX2-1* mutant embryos with and without compounded, conditional loss of *Efnb2*. Dotted yellow lines outline sorted, evaginating *Efnb2*-patterning-negative patches in *NKX2-1*$^{lox/lox}$; *Efnb2*$^{H2B-GFP/+}$; *Foxa2*$^{CreER/+}$ samples (A–C). Yellow arrows indicate unsorted *Efnb2*-patterning-positive cells, and solid red lines outline unsorted *Efnb2*-patterning-negative cells in *NKX2-1*$^{lox/lox}$; *Efnb2*$^{H2B-GFP/lox}$; *Foxa2*$^{CreER/+}$ samples (D–F), illustrating a loss of maintenance of sorting and an abrogation of evagination from *NKX2-1* mosaic mutants upon compounded,

conditional loss of *Efnb2*. (G–R) Immunostaining for LRIG1 (G–J) and *NKX2-1* lineage tracing (K–N) individually and merged with DAPI (O–R) in *NKX2-1*$^{CreER/CreER}$; *ROSA26*$^{Ai75/+}$ mutants and controls at E14.5. Yellow arrows indicate ventral lineage-positive cells intermixing with lineage-negative cells in the dorsal fistula of the mutant, identified by LRIG1 expression.

Scale bars: 50 μm.

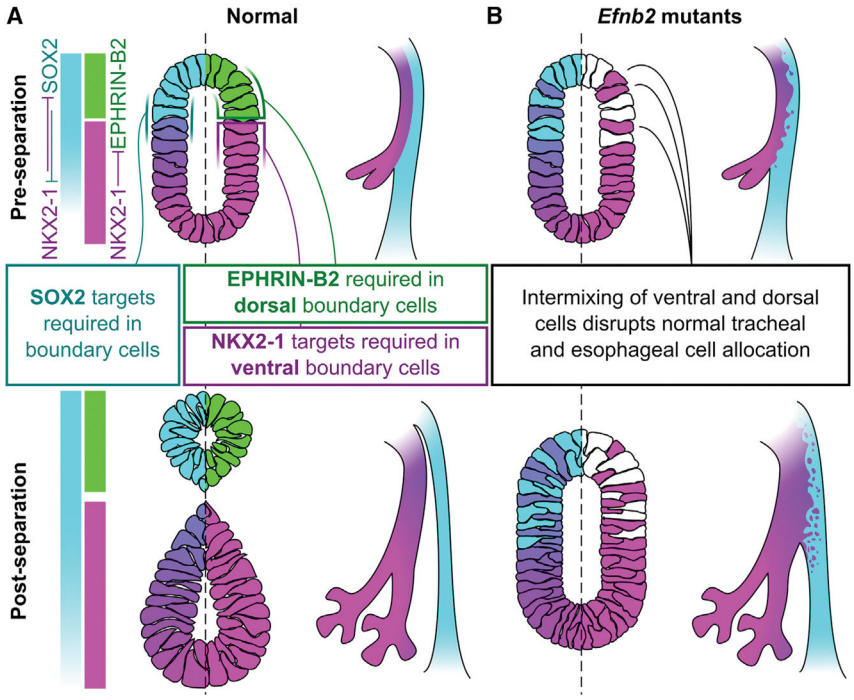

Figure 7. Proposed model for the role of EPHRIN-B2 in TE organogenesis

(A) Induction cues initiate an NKX2-1/SOX2 co-repressive axis. NKX2-1-mediated repression of *Efnb2* restricts EPHRIN-B2 expression to the dorsal, NKX2-1-negative cells. EPHRIN-B2 signaling maintains the NKX2-1 boundary, sorting tracheal-fated cells into their correct domains; TE separation is driven at the EPHRIN-B2/NKX2-1 boundary, requiring EPHRIN-B2 and SOX2; and the two nascent organs proceed with normal development and differentiation.

(B) Upon loss of *Efnb2*, NKX2-1-positive and negative cells intermix, resulting in loss of a sharp dorsoventral TE boundary and disrupting TE separation. Further, in the absence of EPHRIN-B2, NKX2-1-positive cells misallocated to the dorsal foregut contribute ectopic tracheal cell lineages to otherwise esophageal lineage domains.

KEY RESOURCES TABLE

REAGENT or RESOURCE	SOURCE	IDENTIFIER
Antibodies		
Acetylated α-tubulin	Sigma-Aldrich	T7451; RRID: AB_609894
BrdU	Abcam	Ab6326; RRID: AB_305426
Cleaved caspase3	Cell Signaling	9661; RRID: AB_2341188
E-Cadherin	Invitrogen	13–1900; RRID: AB_2533005
EPHA4	R&D	AF641 ; RRID: AB_2099371
EPHB2	R&D	AF467; RRID: AB_355375
EPHB3	R&D	AF432; RRID: AB_2099979
EPHB4	R&D	AF446; RRID: AB_2100105
Phosphorylated EPHA2+A3+A4	Abcam	Ab62256; RRID: AB_942240
Phosphorylated EPHB1+B2	Abcam	Ab61791; RRID: AB_2099832
GFP	Adcam	Ab13970; RRID: AB_300798
Keratin5	BioLegend	905501; RRID: AB_905501
Keratin8	DSHB	AB_531826; RRID: AB_531826
LRIG1	R&D	AF3688; RRID: AB_2138836
Mucin5B	Santa Cruz Biotechnology	Sc-20119; RRID: AB_2282256
NKX2-1	Millipore	07–601; RRID: AB_310743
NKX2-1	Santa Cruz Biotechnology	Sc-8761; RRID: AB_793533
NKX2-1	Thermo-Fisher	MS-699; RRID: AB_142085
RFP	Abcam	Ab62341; RRID: AB_945213
SOX2	Neuromics	GT15098; RRID: AB_2195800
SOX2	Seven Hills Bioreagents	WRAB-1236; RRID: AB_2715498
SOX9	R&D	AF3075; RRID: AB_2194160
Chemicals, peptides, and recombinant proteins		
Tamoxifen	Sigma-Aldrich	T5648
5-Bromo-2′-deoxyuridine	Sigma-Aldrich	B5002
Lipofectamine 2000 Transfection Reagent	Thermo-Fisher	11668027
Critical commercial assays		
RNAScope Fluorescent Multiplex V2 assay	ACDBio/Biotechne	323100
Nano-Glo Dual-Luciferase Reporter Assay System	Promega	N1610
Experimental models: Cell lines		
Mouse: MLE-15	Jeffrey Whitsett, Michael Beers	RRID:CVCL_D581
Experimental models: Organisms/strains		
Mouse: *Efnb2*^{CR}	This lab	MGI:5882571
Mouse: *Efnb2*$^{H2B\text{-}GFP}$	The Jackson Laboratory	MGI:3526818
Mouse: *Efnb2*^{lox}	The Jackson Laboratory	MGI:2176538
Mouse: *Ephb4*^{lox}	Jianping Wu	MGI:5575404
Mouse: *Foxa2*^{CreER}	The Jackson Laboratory	MGI:3774420

REAGENT or RESOURCE	SOURCE	IDENTIFIER
Mouse: *Gata4-G4-Cre*^{Tg}	Anabel Rojas	MGI:4840244
Mouse: *NKX2-1*^{CreER}	The Jackson Laboratory	MGI:5302534
Mouse: *NKX2-1*^{lox}	Holly Ingraham	MGI:3653645
Mouse: *Nkx2–5*$^{IRES\text{-}Cre}$	The Jackson Laboratory	MGI:2448972
Mouse: *ROSA26*^{Ai75}	The Jackson Laboratory	MGI:5603432
Mouse: *ROSA26*^{lacZ}	The Jackson Laboratory	MGI:1861932
Mouse: *ROSA26*^{nTmG}	The Jackson Laboratory	MGI:3716464
Mouse: *Shh*$^{Cre\text{-}EGFP}$	The Jackson Laboratory	MGI:3053959
Mouse: *Sox2*^{CreER}	The Jackson Laboratory	MGI:5295990
Mouse: *Sox2*^{lox}	The Jackson Laboratory	MGI:4366453
Mouse: *Tie2-Cre*^{Tg}	Rong Wang	MGI:3608912
Oligonucleotides		
RNAScope probe: Efna1	ACDBio/Biotechne	428621
RNAScope probe: Epha4	ACDBio/Biotechne	419081
RNAScope probe: Epha7	ACDBio/Biotechne	430961-C2
RNAScope probe: Ephb2	ACDBio/Biotechne	447611
RNAScope probe: Ephb3	ACDBio/Biotechne	510251
RNAScope probe: Ephb4	ACDBio/Biotechne	498201
Recombinant DNA		
pNL1.1.PGK[Nluc/PGK]	Promega	N1441
pNL1.1.TK[Nluc/TK]	Promega	N1501
pGL4.53[luc2/PGK]	Promega	E5011
pGL4.54[luc2/TK]	Promega	E5061